ELSEVIER

NeuroImage

www.elsevier.com/locate/ynimg
NeuroImage 34 (2007) 518–541

Review

Strategies for attenuation compensation in neurological PET studies

Habib Zaidi,[a,*] Marie-Louise Montandon,[a] and Steve Meikle[b,c]

[a]*Division of Nuclear Medicine, Geneva University Hospital, CH-1211 Geneva 4, Switzerland*
[b]*School of Medical Radiation Sciences, Faculty of Health Sciences, University of Sydney, Sydney, Australia*
[c]*Ramaciotti Centre for Brain Imaging, Brain and Mind Research Institute, Sydney, Australia*

Received 20 March 2006; revised 29 September 2006; accepted 3 October 2006

Molecular brain imaging using positron emission tomography (PET) has evolved into a vigorous academic field and is progressively gaining importance in the clinical arena. Significant progress has been made in the design of high-resolution three-dimensional (3-D) PET units dedicated to brain research and the development of quantitative imaging protocols incorporating accurate image correction techniques and sophisticated image reconstruction algorithms. However, emerging clinical and research applications of molecular brain imaging demand even greater levels of accuracy and precision and therefore impose more constraints with respect to the quantitative capability of PET. It has long been recognized that photon attenuation in tissues is the most important physical factor degrading PET image quality and quantitative accuracy. Quantitative PET image reconstruction requires an accurate attenuation map of the object under study for the purpose of attenuation compensation. Several methods have been devised to correct for photon attenuation in neurological PET studies. Significant attention has been devoted to optimizing computational performance and to balancing conflicting requirements. Approximate methods suitable for clinical routine applications and more complicated approaches for research applications, where there is greater emphasis on accurate quantitative measurements, have been proposed. The number of scientific contributions related to this subject has been increasing steadily, which motivated the writing of this review as a snapshot of the dynamically changing field of attenuation correction in cerebral 3D PET. This paper presents the physical and methodological basis of photon attenuation and summarizes state of the art developments in algorithms used to derive the attenuation map aiming at accurate attenuation compensation of brain PET data. Future prospects, research trends and challenges are identified and directions for future research are discussed.

Keywords: Positron Emission Tomography (PET); Brain imaging; Attenuation map; Attenuation compensation; Quantification

Contents

Introduction

The last quarter century has witnessed the introduction of a variety of powerful medical imaging technologies allowing visualization of organ structure and function with exquisite detail. Modern functional brain mapping techniques, such as positron emission tomography (PET), single-photon emission computed tomography (SPECT), functional magnetic resonance imaging (fMRI), electro-encephalography (EEG), magneto-encephalography (MEG), optical imaging and neuroanatomical tools, have been used for assessing the functional organization of the human brain (Gilman, 1998). The specific role of molecular PET imaging in the

* Corresponding author. Fax: +41 22 372 7169.
E-mail address: habib.zaidi@hcuge.ch (H. Zaidi).
Available online on ScienceDirect (www.sciencedirect.com).

1053-8119/$ - see front matter © 2006 Elsevier Inc. All rights reserved.
doi:10.1016/j.neuroimage.2006.10.002

expansion of our understanding of the pathophysiological mechanisms of neurological and psychiatric diseases and in the clinical management of patients is steadily progressing (Jacobs et al., 2003). PET allows *in vivo*, non-invasive three-dimensional (3-D) imaging of regional cerebral blood flow, metabolism and neuroreceptor binding in the brain, amino acid synthesis or amyloid plaques (Heiss and Herholz, 2006). Since functional disturbances occur often earlier than structural ones, a faster and more sensitive detection of pathology is possible, compared with anatomical imaging with, for example structural MRI. During recent years, non-invasive volumetric molecular mapping of brain function with PET has improved markedly through the development of dedicated high resolution instrumentation (Zaidi and Montandon, 2006) and the synthesis of new radiopharmaceuticals (Fowler et al., 2004).

The major challenges to quantitative brain PET when the target is to quantify physiological or pharmacokinetic processes can be categorized in 5 classes (Zaidi and Sossi, 2004):

- Instrumentation and measurement factors: factors related to imaging system performance and data acquisition protocols;
- Physical factors: those related to the physics of photon interaction with biologic tissues;
- Reconstruction factors: issues related to assumptions made by image reconstruction algorithms;
- Physiological factors: factors related to patient motion and other physiological issues;
- Tracer kinetic factors: issues related to difficulties in developing and applying tracer kinetic models, especially at the voxel level.

Quantitative PET imaging requires a variety of skills, resources and personnel beyond what is needed for routine clinical imaging. Neuroscience centres specializing in PET-based brain research are usually populated by multi-disciplinary groups of investigators with backgrounds in neuroscience, chemistry, statistics, mathematical modelling, physics, and computer science. The common goal of these investigators is to develop, test, and validate tools for producing quantitative regional estimates of physiologic or pharmacokinetic parameters from dynamic radiotracer studies. The kinetic analysis can be processed by either applying the radiotracer-dependent model on a pixel by pixel basis, which produces parametric images, or by grouping pixels, representing homogeneous structures, in regions of interest (ROIs). The time course (or time–activity curve) of a single pixel is usually noisy and for some tracers of short half-life it is very difficult to fit the model to the data. The ROI method is more robust since it averages the radioactivity of the pixels included in the ROI, thus allowing to process data with better statistical properties and to reduce computing time since only a few ROIs are analyzed instead of many thousands of pixels. However, it also has limitations particularly when the assumption of tissue homogeneity within a ROI is invalid.

To take full advantage of the quantitative capabilities of PET imaging, patient-specific correction of background and physical degrading factors must be performed (Van Laere and Zaidi, 2005). While most of these corrections are performed using sophisticated computational models, compensation for attenuation relies on consistent assessment of the attenuation map, which is usually derived through an external transmission (TX) scanning apparatus integrated into the PET system design. Two broad classes of method have been used to calculate the attenuation map referred to as "transmissionless" and transmission-based attenuation correction techniques (Zaidi and Hasegawa, 2003). Significant attention has been devoted to optimizing computational performance and to balancing conflicting requirements. Approximate methods suitable for clinical routine applications and more sophisticated approaches for research applications, where there is greater emphasis on accurate quantitative measurements, are being addressed.

Recent developments in high resolution PET instrumentation and the increasing interest in quantitative molecular brain imaging have created a need for a review of the relevance of accurate attenuation compensation strategies in neurological PET studies. Likewise, the number of papers related to this subject published in peer-reviewed journals and presented at various conferences and symposia has been increasing steadily, which motivated the writing of this review as a snapshot of the dynamically changing field of attenuation compensation in cerebral 3-D PET. This paper presents the physical and methodological basis of attenuation correction and summarizes state of the art developments in algorithms used to derive the attenuation map aiming at accurate attenuation correction of brain PET data. This contribution is thus distinct from previous reviews (Bailey, 1998; Zaidi and Hasegawa, 2003; Kinahan et al., 2003b) in the sense that it focuses particularly on brain PET imaging. Future prospects and suggestions for further research will also be discussed. It is recognized that quantification of physiological or pharmacokinetic processes, which is limited by an imperfect "translation" of measurements of radioactivity concentration into quantitative assessments of parameters related to these processes, is still a challenging research topic but falls outside the scope of this review.

Magnitude of attenuation

The physical basis of photon attenuation lies in the natural property that annihilation photons emitted by the positron-emitting radiopharmaceutical interact with human tissue and other materials as they pass through the body. For photon energies representative of those encountered in PET imaging (i.e. 511 keV), annihilation photons emitted can undergo photoelectric interactions where the incident photon is completely absorbed, or more likely, can be scattered following interaction with loosely bound electrons in tissues. Scattering results in a change in the original direction of the incoming photon with (in the case of incoherent or Compton scattering) or without (in the case of coherent or Rayleigh scattering) energy loss. It should be noted that for soft tissue (the major constituent of the body), a moderately low-Z material, two distinct regions of single interaction dominance can be distinguished: photoelectric below and Compton above 20 keV. Furthermore, the percentage of scattered events which undergo Compton interactions in the object is more than 99.7% at 511 keV for water, which renders the number of interactions by photoelectric absorption or coherent scattering negligible. Note that both absorption and scattering are components of the general process of photon attenuation.

In mathematical terms, the magnitude of photon attenuation can be expressed by the exponential equation:

$$\Phi = \Phi_0 \exp\left[-\int_S \mu(s)\mathrm{d}s\right] \quad (1)$$

where Φ_0 and Φ are the incident and transmitted photon fluences (in units of photons per unit area) and ds is a differential of the thickness of tissue encountered as the photon beam passes through the body along path S. The linear attenuation coefficient (μ) represents the probability that the photon will undergo an interaction while passing through a unit thickness of tissue. In other terms, the linear attenuation coefficient is a measure of the fraction of primary photons which interact while traversing an absorber and is expressed in units of inverse centimetres (cm^{-1}).

Fig. 1 shows the narrow-beam attenuation for photons of 511 keV energy as a function of the source depth in soft tissue and cortical bone calculated using photon cross-section data from the XCOM library (Berger et al., 1998) and tissue composition data from ICRU report 44 (ICRU, 1989). It can clearly be seen that attenuation of annihilation photons is severe for positron-emitting radionuclides in singles detection mode. These values also highlight the fact that photon attenuation is an inescapable process, which can affect the image quality and quantitative accuracy of information gathered from PET imaging in a direct and profound way. The mass-attenuation coefficient (μ/ρ) is remarkably similar for all non-bone materials since Compton scatter dominates for these biological tissues. It is worth emphasizing that attenuation

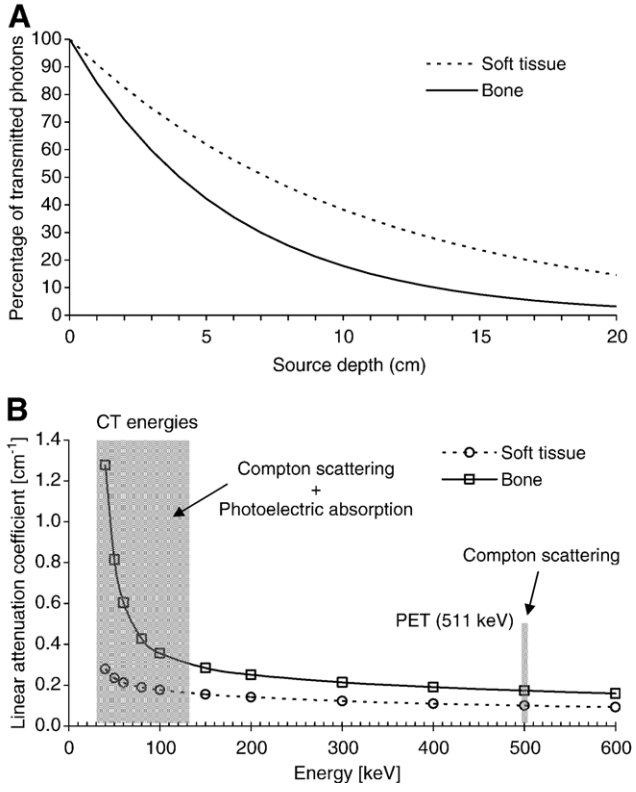

Fig. 1. (A) The narrow-beam attenuation as a function of the source depth for 511 keV photons and different attenuating media illustrating soft tissue which allows greater transmission compared to bone for equal tissue thicknesses. As the source depth is not a useful parameter in coincidence imaging, the curves shown reflect singles detection. (B) Total linear attenuation coefficients versus photon energy for soft tissue and cortical bone computed using the XCOM photon cross-sections database and ICRU report 44 composition data. Note that the ratio of linear attenuation coefficients from for example 70 to 511 keV for water and cortical bone is different (2.01 vs. 2.87) owing to a larger photoelectric fraction caused by the large calcium fraction in cortical bone (~22.4%) (ICRU, 1989).

due to Compton scatter is related to object density whereas photoelectric absorption is related to both density and atomic number. This results in a clear distinction between soft tissue and cortical bone; the latter has more calcium and phosphorus (having higher atomic numbers). Bone has a higher photoelectric absorption cross-section due to presence of calcium. Note also that at the PET energy (511 keV), almost all interactions are Compton scatter.

Depending on the experimental measurement set-up, linear attenuation coefficients can be referred to as either "narrow-beam" in the case where the transmitted photon fluence excludes scattered photons or "broad-beam" otherwise. The "build-up factor" originating from the broad-beam (i.e. uncollimated) conditions of transmission imaging in nuclear medicine is defined as the ratio of the total transmitted photons divided by the ideal narrow-beam (i.e. collimated) measurement corresponding to unscattered photons in the transmitted beam. Consequently, the build-up factor is equal to 1 for narrow-beam geometry but it will increase with depth for broad beam geometries until a plateau is reached. The geometry of the transmission data acquisition system in PET normally guarantees that ideal narrow-beam transmission measurements are obtained. These are required for accurate attenuation correction in PET.

A particularity of PET (in contrast to SPECT) is that the attenuation factor for a given line of response (LOR) depends on the total distance travelled by both annihilation photons within the attenuating medium and is independent of the emission point along this LOR. This makes attenuation correction easier owing to the fact that it only requires a simple pre-multiplication of the emission (EM) data by the resultant attenuation correction factors (ACFs). Yet, the ACFs in PET are huge and quantitation is virtually impossible without compensating for the attenuation effect. The magnitude of the ACFs required in PET might often exceed 100 for some LORs through the body whereas they rarely exceed 10 (typically 3–10) for SPECT (Bailey, 1998).

Importance of attenuation

The fundamental relationship of scatter to attenuation is discussed in Zaidi and Koral (2004). In brief, Compton scatter is the companion of photon attenuation. Specifically, a large fraction of the attenuated photons directly fall into the category of a potential scattered photon. A photoelectric absorption contributes only to attenuation, but a Compton scatter interaction increases attenuation and also sets up a potential scatter corruption. Attenuation and scatter have opposite effects on activity quantification in the sense that photon attenuation decreases counts in high-attenuation tissues, thus allowing too few photons to be detected, resulting in underestimation of activity. In contrast, Compton scatter increases counts in high-attenuation tissues, thus allowing too many photons to be detected, resulting in overestimation of activity. Both uncorrected attenuation and uncorrected scatter corruption cause significant loss of contrast between neighbouring structures and bias in activity quantification. Historically, PET imaging has been performed by obtaining the raw sinograms or projection data, to which one typically applied compensations for image degradations either prior to or after reconstruction. The trend has been to independently compensate for attenuation and for scatter before reconstruction. The motivation behind this is that separation of a complex combined compensation problem into two simpler parts with less computa-

tional burden is often desirable. The scientific community has witnessed an impressive development of computational models for accurate attenuation correction in PET imaging as new approaches of handling scatter and attenuation at the same time are being explored. A recognized attractive property of iterative reconstruction methods is that the algorithm can be modified to incorporate weights or penalties, which reflect the nature of the problem and characteristics of the data acquisition process and scanning system (Comtat et al., 1998). Iterative reconstruction algorithms are commonly used to incorporate corrections for photon attenuation and more recently to compensate for scatter in PET (Zaidi and Koral, 2004). Current attempts to achieve combined compensation are accomplished by taking into account attenuation and scatter during the forward projection step of an iterative reconstruction algorithm, but "putting back" only unscattered photons.

Early attempts to compensate for photon attenuation in PET date back to the time when it was first pointed out as a serious limitation both for qualitative image interpretation and in quantitative analysis (Huang et al., 1979). In the earliest literature on attenuation correction, the main consequence of attenuation was considered to be a loss of image contrast and the creation of erroneously high-count densities in or near low-attenuation regions such as sinus cavities. In the simplest of descriptions, this means that the inherent depression of activity concentration in the centre enhances the activity at the object's boundary resulting in the so-called ring artefact (Zaidi and Hasegawa, 2003). This effect was demonstrated by imaging a uniform distribution of activity in a cylindrical phantom followed by reconstructing the data sets without and with attenuation correction. It was soon after realized that in a clinical setting, since the thickness of tissue varies for different regions of the patient's anatomy, the magnitude of the error introduced by photon attenuation can also vary regionally in the PET image and thus cause a more complicated distortion in at least parts of the image. Therefore, a lesion or activation foci located deep within the body will produce a signal that is attenuated to a greater degree than that for a superficial lesion/foci. Likewise, a tissue region with uniform activity concentration that lies below tissue having a variable thickness will generate an image with variable count density. Consequently, to the extent that clinicians and biomedical researchers desire accurate quantitative images with the finest contrast possible, attenuation is always a problem. The extent to which it can mathematically be shown to have a disabling effect upon the goal for which the image is to be utilized is a much more tricky issue to converse and to document (Bai et al., 2003a). Specific instances will be pointed out in this review where appropriate.

Impact of attenuation correction on clinical neurological PET studies

Image reconstruction without attenuation compensation can introduce severe artefacts into PET images, hence complicating qualitative visual interpretation and causing profound errors when PET images are evaluated quantitatively. For this reason, it is important to understand both the physical processes that underlie photon attenuation and the relative performance of the different methods that can be used to correct PET images for this physical degrading factor. Attenuation compensation in PET is now widely accepted by the nuclear medicine community as a vital component for the production of artefact-free, highly accurate quantitative data. It is worth emphasizing that while the value of the most sophisticated methods available today in clinical practice is no longer the subject of debate in cardiac (Heller et al., 2004) and oncology imaging (Wahl, 1999; Bai et al., 2003a), there are still some controversies regarding their significance in routine clinical brain studies (Zaidi and Sossi, 2004).

Fig. 2 shows a clinical brain PET study reconstructed without attenuation correction and images of the same study corrected for attenuation using measured transmission scanning. The uncorrected image shows typical reconstruction artefacts (depression of activity concentration at the centre of the brain) resulting from the lack of attenuation correction. The literature reporting systematic comparative studies on the effect of different strategies for attenuation correction in brain PET is impressive (see Comparison of methods involving clinical and research studies section). However, there is little in the literature reporting the clinical impact of attenuation corrected images versus no correction. It is well accepted that attenuation correction increases statistical noise.

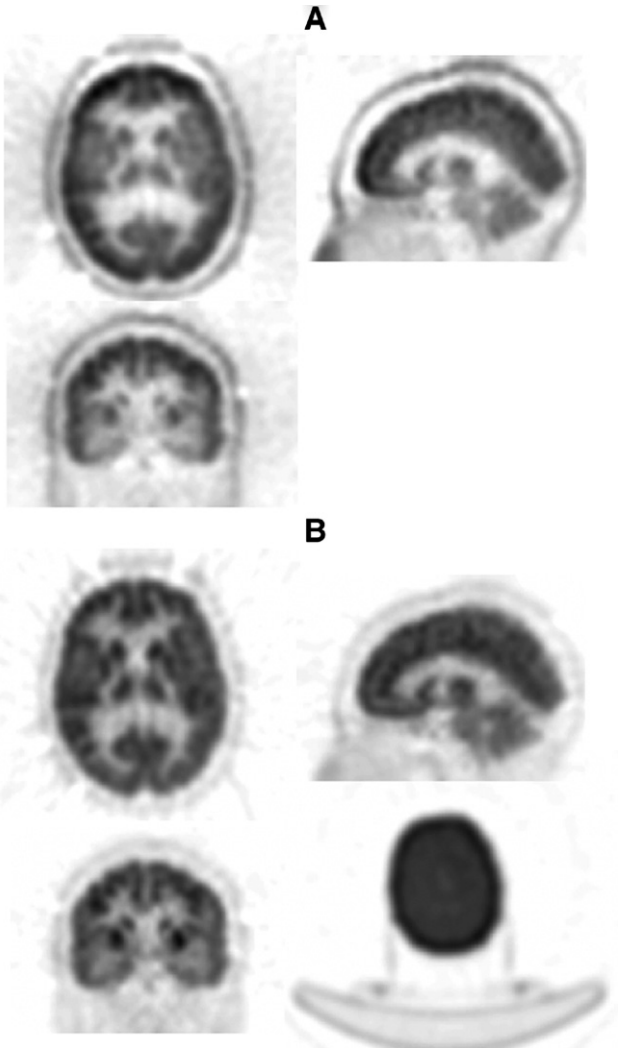

Fig. 2. Filtered backprojection (3DRP) reconstructions of clinical 3D brain PET images presented in different planes without (A) and with attenuation correction (B). A corresponding slice of the attenuation map obtained using measured pre-injection ^{137}Cs transmission scanning is also shown. The non-corrected image tends to depress the reconstructed activity at the centre of the brain. Adapted with permission from SNM (Zaidi and Hasegawa, 2003).

However, in general attenuation compensation recovers the contrast lost and improves quantitative accuracy compared to the case where no correction is applied.

A wide variety of methods have been developed to compensate for photon attenuation in cerebral 3-D PET. In a clinical setting, the balance between algorithmic complexity and the validity of results obtained is an important criterion when selecting an attenuation correction technique. Even though the methods which make a large number of assumptions can frequently be undemanding, it is not necessarily true that complex algorithms will always perform better. The extra complexity must be used judiciously and justified for the particular application at hand. In many cases, extra complexity can just as easily result in unreliability as in improved results. In the clinical setting, it has become standard practice to use simplified techniques compared to the often complex methods developed for research where there is greater emphasis on quantitative accuracy. The simplest method consists of approximating the object outline by an ellipse drawn around the edges of the object followed by assignment of a uniform attenuation coefficient within the contour to generate the attenuation map. An irregular contour can also be drawn manually by a qualified technologist or computed using automated edge detection techniques. The method is generally appropriate for brain studies and is implemented on virtually all commercial PET systems. Although empirical, the method has some attractive properties, namely speed, simplicity, and increased patient throughput, which is a relevant issue in a busy clinical department.

Measured transmission-based attenuation correction is the most commonly used procedure both in clinical and research settings since it is expected to yield the best attenuation map as a result of matched energy and spatial resolution (Ostertag et al., 1989; Hooper et al., 1996; Zaidi et al., 2004). However, motion-induced misalignment between TX and EM scans can result in erroneous estimation of regional tissue activity concentrations (van den Heuvel et al., 2003). Likewise, the high cost of dual-modality PET/CT units and the potential introduction of artefacts in the presence of contrast media (Ay and Zaidi, 2006b) or metallic dental implants (Kamel et al., 2003) when using CT-based attenuation correction (CTAC), thus biasing quantitative PET estimates and disturbing the visual interpretation of PET images, are major limitations for brain imaging dedicated facilities. The search for reduction of acquisition time in brain PET scanning protocols spurred the development of transmissionless algorithms for derivation of the nonuniform attenuation map, thus eliminating the need for acquisition of a measured transmission scan (Watabe et al., 2001; Weinzapfel and Hutchins, 2001; Zaidi et al., 2003, 2004; Montandon and Zaidi, 2005).

Methods for determination of the attenuation map in neurological PET studies

The accuracy achieved by attenuation correction procedures depends mainly on the rigour followed to derive the patient-specific attenuation map. Two broad classes have emerged: (i) calculated (transmissionless) methods, which are based on an assumed anatomical model representing the shape and spatial distribution of attenuation coefficients in the head and (ii) measured (transmission-based) methods, which in general rely on supplementary acquisition of a transmission scan. These techniques vary in complexity, accuracy, and computation time required.

Approaches that do not require a transmission scan

As reported earlier, the use of transmission-based nonuniform attenuation correction introduces the least bias and can supply more accurate absolute quantification as compared to calculated attenuation correction and therefore constitutes the gold standard in cerebral 3-D PET imaging. However, the need to acquire an additional transmission scan complicates the scanner design and is a restrictive factor since it represents a substantial increase in the overall acquisition time, thus decreasing patient comfort and patient throughput, indirectly increasing the costs of PET exams (Fig. 3). More importantly, elimination of the TX scan results in reduction in overall radiation absorbed dose to staff and patients, a significant issue when dealing with human volunteers participating in research protocols. While keeping the total acquisition time constant, simultaneous EM/TX (SET) scanning requires great care in its implementation in order to avoid cross-contamination problems (see Radionuclide-based transmission scanning section). It should be noted that a waiting period between the transmission and the (static) emission scan is only needed for some clinical studies (mainly FDG). In the standard practice for brain research studies, a transmission scan (typically 10 min) is performed just prior to a dynamic emission scan (typically 60–90 min).

A recent study compared the difference between ^{68}Ga/^{68}Ge- and CT-based transmission scanning using a combined PET/CT device in terms of radiation burden to the patients during brain, cardiac and whole-body scans by using a Rando Alderson phantom and thermoluminescent dosimeters (Wu et al., 2004). The authors reported negligible effective dose equivalents (EDEs) for brain transmission scanning (0.03 mSv) when using ^{68}Ga/^{68}Ge rod sources, while EDEs of 0.22 mSv in the high-speed mode (pitch of 6:1) and 0.45 mSv in the high-quality mode (pitch of 3:1) were measured for brain CT-based transmission scans for a tube current of 80 mA and a tube rotation time of 0.8 s on the Discovery LS system (GE Healthcare Technologies, Waukesha, WI, USA). This range is obviously negligible compared to dosimetry of typical brain PET emission scans using ^{18}F-FDG or ^{11}C-raclopride where EDEs have been reported as 10.73 mSv (Deloar et al., 1998) and 3.23 mSv (Slifstein et al., 2006), respectively, for an injected activity of 370 MBq for an adult.

Calculated methods

Alternative methods of attenuation correction were sought to overcome the limitations of transmission scanning observed during the early stages of PET development. These included noise propagation from the transmission scan to the attenuation-corrected emission scan (Dahlbom and Hoffman, 1987) and the time required to perform a statistically reliable transmission scan, thus extending the overall study time and making patient movement more likely. It should be noted that most of these limitations have since been overcome with the development of rod-windowed transmission devices and post-injection transmission scanning methodology. However, these approaches were not available during the first two decades of PET development.

An initial approach to calculated attenuation correction involved performing a preliminary reconstruction of the emission data without attenuation correction and then drawing an elliptical ROI that defined the outline of the head on each transverse slice (Huang et al., 1979, 1981). This approach is refereed to here as calculated attenuation correction using a manually defined contour (CAC_m).

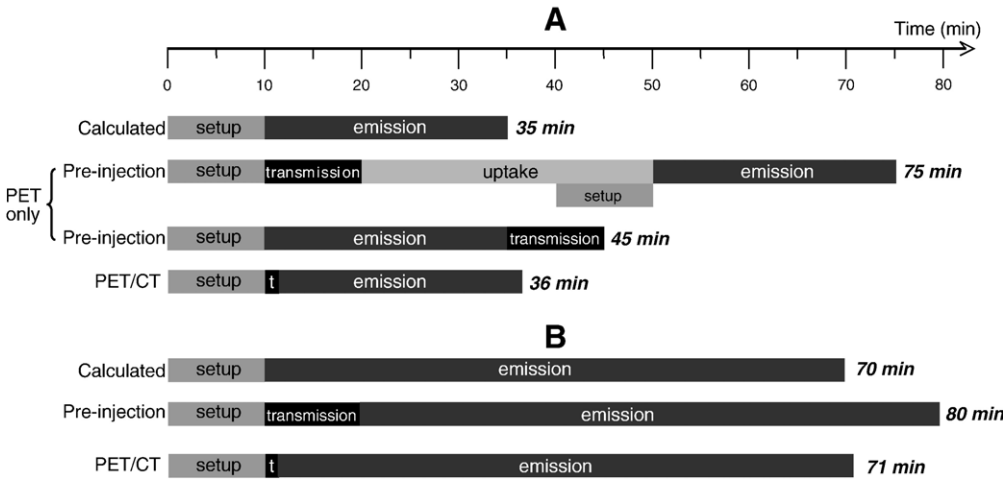

Fig. 3. Comparison of total camera time for different data acquisition protocols in cerebral PET scanning using both calculated and measured pre- and post-injection transmission-based attenuation correction protocols. It can be seen that a waiting period between the transmission (typically 10 min) and the (static) emission scan (25 min in this example) is only needed for some (mainly FDG) clinical studies (A). In the standard practice for brain research studies (B), a transmission scan is performed just prior to a dynamic emission scan (60 min in this example).

The ACFs were then calculated for each LOR passing through the head assuming a constant linear attenuation coefficient, μ:

$$\mathrm{ACF} = \exp(\mu l) \tag{2}$$

where l is the length of the chord that forms the intersection between the LOR and the ellipse. After calculating the ACFs for every LOR, the measured emission projections are multiplied by the ACFs and reconstructed to form attenuation corrected images. The main drawbacks of this technique are the time required to draw each ROI (more of a problem on current generation multi-slice scanners than on the early 1–3 slice brain scanners), operator dependence of the results and bias caused by the fact that the head is not perfectly elliptical, nor does it have uniform density.

Various refinements to the method of calculated attenuation correction were developed to improve its practical utility and accuracy. The first advance occurred when Bergstrom et al. (1982) developed a method of calculating the chord lengths (hence, the ACFs) directly on the projections, thus eliminating the initial reconstruction step. This method also allowed for the differing densities of the skull and brain and assumed a certain constant thickness for the skull. However, the method still assumed that the head has an elliptical outline in each transverse slice. Several investigators subsequently improved the automated approach by developing sophisticated edge detection algorithms that operate on the emission projections and make no assumption about the geometric shape of the head (Tomitani, 1987; Michel et al., 1989; Siegel and Dahlbom, 1992). Indeed, the method by Siegel and Dahlbom (1992) was able to accommodate parts of the head at the skull base that have a concave outline rather than a convex one. This approach is refereed to here as calculated attenuation correction using an automatically defined contour ($\mathrm{CAC_a}$).

A more sophisticated fully automated technique was proposed by Weinzapfel and Hutchins (2001) to work out a three-component (brain, skull and scalp) model of the attenuation map. An estimated skull image is generated by filtered backprojection of the reciprocal of an emission sinogram. The thickness and variable radius of the skull is estimated from profiles extracted from the image. The resulting thickness and radius values are then used to generate a model of the brain, skull, and scalp. Scaled linear attenuation coefficients determined empirically by fitting the emission-derived head model to measured transmission data in human subjects are then assigned to each brain structure to generate an attenuation map for the head. Despite progress made, the main limitation of calculated attenuation maps is the fact that values for the linear attenuation coefficients of tissues have to be assumed. Different approximations were adopted for assignment of attenuation coefficients to brain tissue and skull in addition to the constant thickness for the latter. Table 1 summarizes linear attenuation coefficients reported in the literature for different attenuating tissues encountered in cerebral PET scanning when using calculated attenuation correction techniques (Zaidi et al., 2003). The assumptions made regarding the skull thickness are also shown. With these refinements, calculated attenuation correction is reasonably accurate (but the readers attention is drawn to specific problems discussed in Comparison of methods involving clinical and research studies section) and still frequently used in neurological PET studies as an alternative to transmission-based approaches.

Atlas-guided methods

It has been shown that invalid assumption of tissue uniformity might lead to significant bias in activity quantification, especially in regions of high variability, such as air cavities and nasal sinuses. The advantages of calculated methods and the limitations of the approaches described above spurred the development of a new class referred to here as template or Atlas-guided attenuation correction (AGAC) techniques, where this problem is overcome by inferring anatomy from a head atlas. The method developed by Stodilka et al. (2000) called inferring-attenuation distributions consists of deformably registering the brain component of a digitized head atlas derived from a voxel-based head model obtained by segmenting high-resolution MRI of a single subject (Zubal et al., 1994) to SPECT images. The attenuation map is derived by registering the functional brain component of the head phantom having a source distribution with appropriately scaled specific activities of the gray matter, white matter and ventricles, to

Table 1
Summary of linear attenuation coefficients (in cm^{-1}) reported in the literature for different tissues of the head used for attenuation correction purposes in brain PET studies

Linear attenuation coefficient (cm^{-1})			Skull thickness (mm)	Reference
Brain tissue	Skull	Nasal sinuses		
0.0960	0.151	na [a]	4.5	(Bergstrom et al., 1982)
0.0940	0.171	na	8	(Tomitani, 1987)
0.0880	0.157	na	6% of the outer contour	(Michel et al., 1989)
0.0950	0.151	na	5	(Siegel and Dahlbom, 1992)
0.0990	0.136	na	ps [b]	(Weinzapfel and Hutchins, 2001)
0.0993	0.143	0.0536	ps	(Zaidi et al., 2003)

The assumptions made regarding the skull thickness are also shown. Adapted from Zaidi et al. (2003).
[a] Not applicable.
[b] Patient-specific.

a preliminary PET reconstruction of the patient and then applying the resulting spatial transformation to the anatomical head atlas. The technique was also later extended and implemented successfully for brain PET imaging (Zaidi et al., 2004). However, several investigators reported that a major limitation of the Zubal head phantom is that the sinus is larger than usual (Arlig et al., 2000; Stodilka et al., 2000; Zaidi et al., 2004). It was also hypothesized that new phantom models based on average patient populations may not help to solve this problem owing to the large variability in size and shape of the frontal sinus among patients. In addition, the simplicity of the registration algorithm used (7 parameters global rescaling model) and the crude approximations relating to the spatial distribution of the tracer is another severe constraint which needed further enhancement.

More refined methods suffering from the limitations discussed above make use of an optical tracking system to derive a 3-D patient-specific head contour (Watabe et al., 2001), where a previously acquired reference attenuation map of a single subject is transformed to match the contour of the reference head with the target head using the thin plate spline technique. A practical advantage of the optical tracking system is that it can also be utilized for motion correction. Taking advantage of the wider availability of both transmission and tracer-specific (e.g. ^{18}F-FDG) emission atlases based on average patient populations (rather than relying on an atlas based on a single subject and a hypothetical tracer distribution), the feasibility of Atlas or template-guided attenuation correction in cerebral 3-D PET imaging has been recently proposed and validated in a clinical environment using both voxel-based (Statistical Parametric Mapping − SPM) (Montandon and Zaidi, 2005) and volume of interest (VOI)-based (Montandon and Zaidi, in press) analysis. In this case, the patient-specific attenuation map is derived by non-linear warping of a transmission template constructed by scanning a representative population of healthy subjects. Fig. 4 shows a diagram summarizing the general principles of the algorithm and main steps required to generate a patient-specific attenuation map from emission and transmission templates. The accuracy of the algorithm depends to a great extent on the performance of the coregistration and anatomic standardization techniques applied to the tracer-specific emission template to match the patient data (Hosaka et al., 2005).

The fundamental issue that needs to be addressed when using this approach is the level of accuracy one can achieve for depicting the global anatomy using an Atlas constructed from a normal database to predict the individual attenuation map. A recognized important conceptual limitation for this technique is the existence of patient-specific anomalies that are not modelled in an atlas

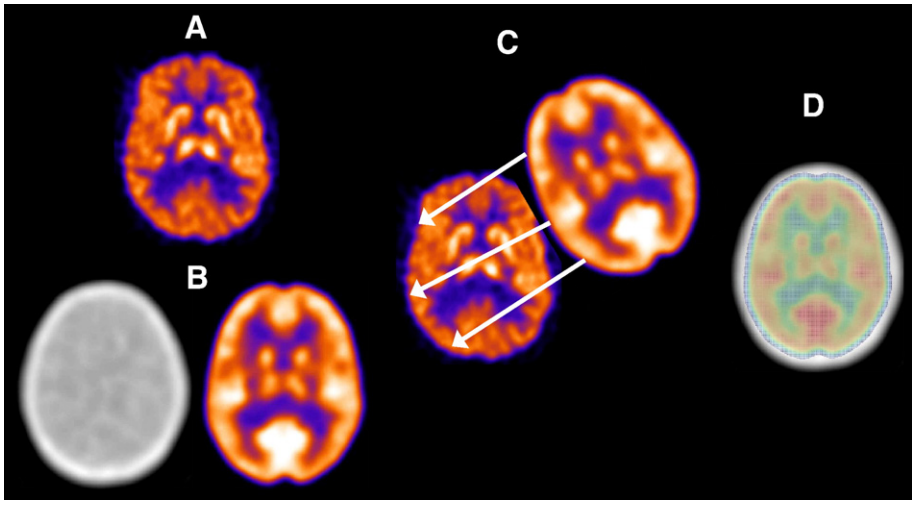

Fig. 4. Illustration of the principle of Atlas-guided derivation of the attenuation map (Montandon and Zaidi, in press). (A) Preliminary PET reconstruction obtained using calculated attenuation correction. (B) ^{18}F-[FDG] emission and transmission templates. (C) Emission template is spatially normalized to preliminary PET reconstruction. (D) Application of same transformation to transmission template.

obtained from an average representation of the population. Standardizing patient brain images in a clinical setting should therefore be performed with caution. For instance, the use of automated algorithms is known to fail in the presence of a focal perfusion or metabolic lesion, especially when nonlinear transforms are utilized. These algorithms cause considerable and inappropriate image distortion when attempting to reduce image mismatch between patient image and template at the site of the lesion. To overcome this hurdle, Brett et al. (2001) suggested to use cost-function masking, thereby excluding the lesion areas used in the calculation of image difference, so that the lesion does not bias the transformations. Preliminary investigations have shown that this approach can yield excellent results provided that the lesion size/location is known *a priori* (Stamatakis et al., 2001). However, there is a rather important conceptual limitation for this approach, namely the lack of automated techniques for determination of the masked-out regions, when lesion location is not known *a priori*. This issue remains an open question which requires further research and development efforts.

Another limitation of most calculated attenuation correction methods is that they do not take into account the frontal sinus, attenuation in the bed, and head holder having attenuation properties different from those of brain tissue as well as possible other auxiliary equipment that might be in the field of view for some applications. There is large variability in size and shape of the frontal sinus among subjects. Theoretical modelling of bed and head support attenuation which result in underestimation of activity concentration of the posterior part in the brain (Bettinardi et al., 1994) can be modelled through assignment of fixed theoretical known attenuation coefficients for these objects. The exact position of the acrylic head holder is, however somewhat flexible and thus difficult to reproduce for each subject. The most accurate way is to model these features using measured transmission. A potential procedure consists in acquiring a good statistics transmission bed and head holder scan followed by image reconstruction using an algorithm similar to the protocol used for patient transmission scans. The low noise image of the bed can be added up to the derived attenuation map by reading from the header files of PET emission and bed images the vertical position of the bed and making appropriate adjustments to account for the different bed elevations between the bed scan and the clinical brain scan. Similar procedures also were reported for the head support (Bettinardi et al., 1994).

Other sophisticated methods

More ambitious techniques for transmissionless attenuation correction aim at reconstructing the attenuation map directly from the emission data. This approach was pioneered by Censor et al. (1979), where alternating iterations of the reconstruction algorithm were used to reconstruct emission images and attenuation maps from a set of emission projections alone. This was followed by seminal contributions by Natterer (1993) giving further confidence in the potential feasibility of this approach. Several investigators applied various optimization techniques based on similar philosophies to generate emission images and attenuation maps (Zaidi and Hasegawa, 2003). For instance, Nuyts et al. (1999) formulated the problem as an optimization task where the objective function is a combination of the likelihood and an *a priori* probability. The latter uses a Gibbs prior distribution to encourage local smoothness and a multimodal distribution for the attenuation coefficients. Other approaches include the use of the EM algorithm (Glatting et al., 2000; Krol et al., 2001), or penalty functions (Dicken, 1999; Kaplan et al., 1999). The techniques have had limited success, but often produce artefacts in the form of cross-talk between the emission image and the attenuation map.

Other transmissionless reconstruction methods attempt to avoid cross-talk between the emission image and attenuation map by reconstructing the emission image and the attenuation map separately. A more general technique applies the consistency conditions for the range of the attenuated Radon transform to obtain the attenuation map from emission data (Natterer, 1993, 2001). Implementations based on previously used continuous conditions have shown that reconstructions did not converge to an acceptable solution. Bronnikov (1999, 2000) suggested an original approach that strengthens the paradigm of the consistency conditions by setting them in the framework of a discrete representation of the problem. It should be noted that even though much valuable research efforts have been carried out in this area, there is no clear evidence in the literature substantiating the applicability of these techniques in a clinical environment. Further research is clearly needed to convince the nuclear medicine community and gain confidence in this approach. Potential future developments are addressed in Summary and future directions section below.

Measured transmission-based approaches

In clinical and research settings, one needs to accommodate situations of nonuniform attenuation for which the spatial distribution of attenuation coefficients is not known *a priori*. To date, the most accurate means of determining a patient-specific attenuation map are based on measured transmission scanning protocols acquired before (pre-injection), during (simultaneous), or after (post-injection) the emission scan. This includes radionuclide-based transmission scanning, approaches requiring segmented MR images or appropriately scaled X-ray CT scans acquired either independently on standalone PET cameras or simultaneously on dual-modality PET/CT imaging systems. Several transmission scanning geometries have emerged for clinical implementation on dedicated PET units as illustrated in Fig. 5. The following sections describe the different transmission sources and data acquisition geometries that have been proposed so far.

Radionuclide-based transmission scanning

The first, and still most widely used, method of attenuation correction in PET is based on a separate transmission scan of the area to be imaged prior to administration of the radiopharmaceutical to the subject. This is sometimes referred to as pre-injection transmission scanning, or measured attenuation correction (MAC_{pre}). The early PET scanners used transmission ring sources of the positron-emitting radionuclides $^{68}Ga/^{68}Ge$ ($T_{1/2}$=68 min and 270.8 days, respectively), which co-exist in secular equilibrium (Zaidi and Hasegawa, 2003). The second generation PET scanners typically used one or more rod transmission sources, containing up to 400 MBq of a long-lived isotope such as ^{68}Ge ($T_{1/2}$=270.8 days) which decays to the positron emitter ^{68}Ga ($T_{1/2}$=68 min). The source(s) would rotate around the edge of the field of view recording coincidences between detectors on the near and far sides of the subject. A separate scan using the same source(s) would be performed while there is no subject in the field of view. The coincidences recorded during this so-called blank scan are divided

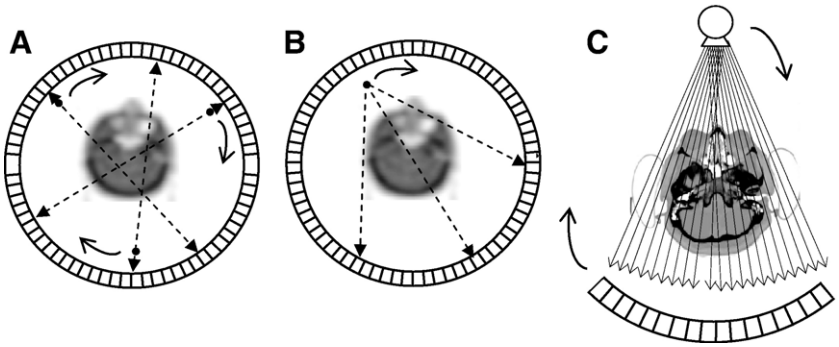

Fig. 5. Different configurations of transmission scanning geometries for PET are shown in the diagram. (A) Rotating positron-emitting rods measuring transmission in coincidence mode, (B) single-photon source producing coincidence events between the known source position and photons detected on the opposing side of the detector ring, and finally (C) rotating X-ray tube for a typical helical CT design integrated in current generation dual-modality PET/CT scanners.

by those recorded during the transmission scan to give the ACFs for each LOR:

$$\mathrm{ACF} = \frac{\text{blank}}{\text{transmission}} = \frac{C_0}{C_0 \exp\left(-\int_{L(s,\phi)} \mu(x)\mathrm{d}x\right)} = \exp\left(\int_{L(s,\phi)} \mu(x)\mathrm{d}x\right) \quad (3)$$

where C_0 is the blank count rate recorded at the current LOR, $\mu(x)$ is the linear attenuation coefficient at position x in the body and $L(s,\phi)$ is the integration path along the LOR.

In theory, attenuation correction could be affected by multiplying the emission projections by the ACFs on a LOR-by-LOR basis without further processing. In practice, this leads to substantial noise propagation into the corrected emission data because of the typically poor signal-to-noise ratio of transmission measurements made with a positron emitter (Dahlbom and Hoffman, 1987). This occurs because the denominator in the equation above becomes very small when either the density of tissue is great or the distance in tissue through which photons pass is large and because transmission data obey Poisson statistics (as do all radiation measurements). To overcome this problem, the transmission and blank scans are normally smoothed using a low-pass filter before calculating the ACFs.

The transmission-based approach is sometimes considered the gold standard of attenuation correction methods, although it is an imperfect one. First, total imaging time is increased and the technique suffers from image registration problems caused by patient misalignment or motion (van den Heuvel et al., 2003). Second, as pointed out above, it propagates noise, particularly in LORs that pass through the centre of the head and the thickest parts of the skull (e.g. the skull base). Third, the filtering that is normally applied to overcome this, results in a difference in spatial resolution between the processed transmission data and the emission data to which it is applied, since emission data are not normally smoothed at this stage. This results in bias at the interfaces between regions of high and low tissue density (Palmer et al., 1986; Meikle et al., 1993) and is more of a problem in whole body PET, where tissue density is more heterogeneous, than in neurological studies.

To limit head movement, light restraints are used in many institutions to minimize motion artefacts. For accurate repositioning of patients for the emission scan, thermoplastic face masks are also used in some facilities (Fig. 6). In addition, with the advent of dedicated high resolution PET scanners, methods are under development to monitor and correct for patient motion and misregistration between transmission and emission scans as small amounts of motion can cause significant blurring and loss of quantitative accuracy in the images (Bloomfield et al., 2003). Conventional motion compensation algorithms rely on extraction of the motion information from the emission data itself though the accuracy of this approach is limited by the noisy nature of the emission data. Advanced methods, make use of external real-time external motion tracking systems. Various multi-acquisition frame and event-by-event image-based and projection-based correction methods have been proposed and evaluated (Tellmann et al., 2006). As an observation, a general theme in motion compensation algorithms is seen to be the use of increasingly sophisticated software to make use of existing advanced hardware. In this sense, this field is very open to future novel ideas (hardware, and especially software) aimed at improving motion detection, characterization and compensation. It was reported that reducing the mismatch between transmission and emission scans through

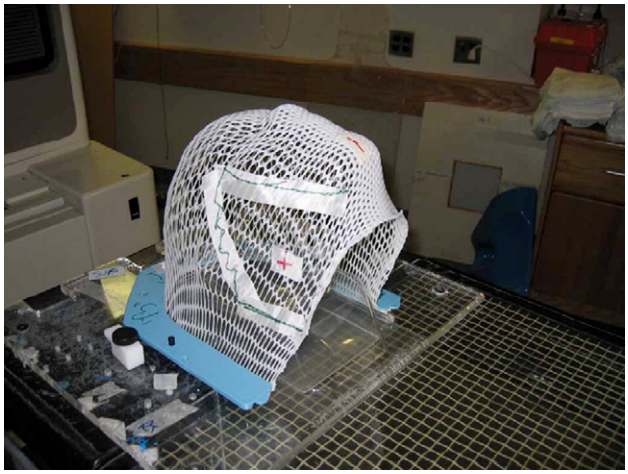

Fig. 6. Illustration of the head fixation system consisting of a thermoplastic face mask used in the first author's department to limit head motion and to allow accurate repositioning of patients for the emission scan following the pre-injection transmission scan.

image registration results in an increase in signal-to-noise ratio (van den Heuvel et al., 2003).

To improve counting statistics, a single photon emitting point source can be used as a transmission source (deKemp and Nahmias, 1994; Karp et al., 1995). LORs are formed between the known location of the point source as it rotates around the subject and the detector on the far side that absorbs the transmitted photons. This is a far more efficient process than counting coincidences between the annihilation photons emitted by a positron source which requires both photons to be absorbed in their respective detectors. The result is considerably improved signal-to-noise ratio in ACFs derived from single photon emitters compared with those derived from positron emitters (Bailey, 1998). Single-photon emitting transmission sources have the further advantage that isotopes can be chosen that emit photons at an energy different from the 511 keV of annihilation photons. This makes it possible to acquire transmission data after the radiopharmaceutical has been administered to the subject. For example, if ^{137}Cs ($T_{1/2}$=30.04 years) is used, there is little interference between the 662 keV photons emitted by the transmission source and the 511 keV annihilation photons emitted from the subject by the radiopharmaceutical. The TX data are usually normalized to a slab phantom scan and corrected for scatter and cross-section variation using a log-linear transformation of the attenuation factors (Watson et al., 1999). Various approaches have also been proposed to eliminate contamination of emission data by transmission photons and to reduce spillover of emission data into the transmission energy window (Zaidi and Hasegawa, 2003). For example, it has been demonstrated on the High Resolution Research Tomograph (HRRT) PET scanner that emission contamination can lead to gross underestimation of tissue attenuation. It was also reported that the most accurate way to compensate for this is to combine nonuniform emission contamination subtraction with transmission image segmentation (de Jong et al., 2004).

The possibility to perform post-injection transmission (MAC_{post}) scanning is not limited to single-photon emitting transmission sources. A technique called rod windowing was introduced in the 1980s which allows the vicinity of measured coincidence LORs to the transmission source(s) to be recorded (Carroll et al., 1983; Huesman et al., 1988; Kubler et al., 1988; Ranger et al., 1989; Jones et al., 1995; Luk et al., 1995). The source location is continuously encoded and projection elements representing collinear, or nearly collinear, detector pairs are identified and discriminated from those that are not. Coincidences recorded in a narrow window centred on each rod source (primarily transmission events) are stored separately from those recorded outside the window (primarily emission events). Methods were developed that take these separately stored events and correct for the minor emission contamination of transmission measurements recorded within the window, thus allowing transmission scanning to be performed following tracer administration (Carson et al., 1988; Daube-Witherspoon et al., 1988; Hooper et al., 1996).

The rod windowing technique was extended to allow EM and TX scans to be performed simultaneously (MAC_{set}) (Thompson et al., 1991; Meikle et al., 1997). This approach has been used routinely by some centres for attenuation correction of whole-body FDG PET studies, where the transmission scan would otherwise occupy a significant proportion of the time the subject is on the bed (Meikle et al., 1995; Lodge et al., 1998). In neurological PET studies, although the technique has been validated for both clinical and research protocols, it is not routinely used, mainly because the impact on study duration is less than in whole body PET. More recently, a simultaneous emission–transmission scanning system has been developed that reduces contamination of the emission data by the emitted transmission photons using a fast, dedicated, lutetium oxyorthosilicate (LSO)-based reference detector placed close to the collimated coincidence point source used to produce the transmission data (Watson et al., 2001). The preliminary results were very encouraging demonstrating good transmission image quality for low activity concentrations of the tracer (<2.5 kBq/ml), but significant degradations were observed for higher emitter concentrations.

Noise propagation from the short transmission to the emission scans during the attenuation correction process is an important issue to consider especially for dynamic scanning protocols which are characterized by significantly higher noise properties compared to typical static imaging where the acquisition time is longer. It has been demonstrated that low count transmission scans (poor statistics) resulted in biased quantification (Freedman et al., 1996). Therefore, high quality transmission scans are essential in the case of quantitative dynamic PET studies.

To avoid lengthy transmission scans, techniques using transmission image segmentation or segmented attenuation correction (SAC) and tissue classification have been proposed to reduce noise propagation from transmission to emission scans by delineating different anatomical regions of uniform attenuation followed by assignment of known tissue-dependent attenuation coefficients using weighted averaging. The segmented attenuation maps are then forward projected to generate less noisy ACFs to be used for attenuation correction of the corresponding emission data. In a clinical setting, segmentation algorithms must be designed to balance image quality and required algorithmic complexity and resulting computational time.

Most transmission image segmentation algorithms fall into one of the following two classes: histogram-based thresholding techniques (Meikle et al., 1993; Xu et al., 1996; Bilger et al., 2001) and fuzzy-clustering based segmentation techniques (Bettinardi et al., 1999; Zaidi et al., 2002). Thresholding-based techniques use the gray-level histogram counts to distinguish between regions. Since only intensity information is used for the segmentation, this often results in noisy segmentations and the technique most likely fails in regions where the total number of counts is small (e.g. the skull) since the classification is based solely on the characteristics of the histogram. Therefore, the performance of such techniques strongly depends on the choice of the thresholds. In contrast, fuzzy-clustering based segmentation techniques have proved to be more robust as automated, unsupervised algorithms for segmenting noisy images for different applications. These are iterative approaches that minimize an objective function requiring the number of clusters as input parameter to assign a membership degree to all voxels with respect to a cluster centre.

Other attractive approaches to segment noisy transmission data include the use of active contour models (Tai et al., 1996), neural networks (Yu and Nahmias, 1996), morphological segmentation (Riddell et al., 1999), and hidden Markov modelling (Anderson et al., 2002). An alternative to segmentation of transmission images with the goal of reducing noise in PET transmission measurements includes Bayesian image reconstruction (Fessler et al., 1997; Alenius et al., 1999) and non-linear Gaussian (Kitamura et al., 2000) or anisotropic diffusion (Demirkaya, 2002) filtering.

X-ray-based transmission scanning

Attenuation maps generated for attenuation correction of PET emission data have been traditionally obtained using conventional external radionuclide sources. Conceptually, the procedure is analogous to the principle of X-ray CT imaging where the radiation emanating from a rotating X-ray tube is transmitted through the patient's body and recorded by an array of detector elements on the opposite side. A tomographic reconstruction algorithm can then be used to calculate the spatial distribution of attenuation coefficients. On commercial CT scanners, the reconstructed intensities are usually represented in terms of normalized (to water) "CT numbers" or "Hounsfield units" (HU), named after Godfrey Hounsfield, an established pioneer of CT. Yet, the pixel values are directly related to the linear attenuation coefficient (μ) at the same point in the patient, calculated for the effective energy of the photon beam used to generate the CT image:

$$\text{CT number} = \frac{\mu - \mu_{H_2O}}{\mu_{H_2O}} \times 1000 \quad (4)$$

Note that with this definition, air and water have a CT number of −1000 HU and 0 HU, respectively.

Consequently, the fact that a low noise X-ray CT image is used to generate a patient-specific attenuation map for correcting the PET emission data for photon attenuation is not surprising. In addition, X-ray CT images provide an anatomical context that interpreters use to differentiate normal tracer uptake from that indicating disease, and to help localize disease sites within the body.

In a clinical setting, this can be accomplished by sequential scanning of the patient either separately on standalone PET and CT scanners or on a combined PET/CT scanner. For the former, the challenging issue of image registration should be performed using off-line image registration software, with or without the help of external fiducial markers (Hutton and Braun, 2003). Multimodality coregistration algorithms work relatively well and can be applied most successfully to neurological studies, where the skull provides a rigid structure that maintains the geometrical relationship of structures within the brain. In contrast, off-line image registration is more difficult to perform accurately in whole-body imaging where organs can flex and bend making it difficult to maintain a consistent anatomical configuration.

Dual-modality PET/CT units offer a critical advantage over separate PET and CT imaging systems in correlating functional and anatomical images without moving the patient (other than table translation). This technique thereby produces anatomical and functional images with the patient in the same position and during a single procedure, which simplifies the image registration and fusion processes (Townsend and Cherry, 2001). PET/CT systems have demonstrated their ability to facilitate attenuation correction using an X-ray based patient-specific attenuation map that can be produced faster and more accurately than attenuation maps generated with external radionuclide sources (Hasegawa and Zaidi, 2005). Many investigators explored the possible application of these techniques in SPECT (Nickoloff et al., 1984; Fleming, 1989; LaCroix et al., 1994; Blankespoor et al., 1996). Likewise, the feasibility of CTAC in PET was demonstrated (Kinahan et al., 1998). Nevertheless, a number of pitfalls arise from the use of CT to generate attenuation maps for correction of the PET data that must be considered to avoid typical artefacts that are unique to PET/CT imaging.

As mentioned above, X-ray CT inherently provides a patient-specific measurement of the linear attenuation coefficient at each pixel in the CT image. Usually the high resolution anatomical images are first down-sampled following by Gaussian filtering to match the resolution of the PET data. However, the linear attenuation coefficient measured with CT is calculated at the effective energy of the X-ray beam rather than at the energy of the annihilation photons emitted by the positron emitting radiopharmaceutical during the emission study. A precise conversion of CT numbers derived from low-energy polyenergetic X-ray spectra to linear attenuation coefficients at 511 keV is thus essential. Several strategies have been devised for calibrating the CT image for attenuation correction of the PET emission data including scaling (Beyer et al., 1994), segmentation (Kinahan et al., 2003a), hybrid segmentation/scaling (Kinahan et al., 1998), piece-wise linear scaling (Burger et al., 2002; Bai et al., 2003b), and dual-energy decomposition methods (Guy et al., 1998). It should be noted that most commercial PET/CT scanners use the bilinear calibration curve method, which is generally calculated at a preset tube voltage (120–140 kVp) and tube current. The effect of tube current (Kamel et al., 2002; Ay and Zaidi, in press) and tube voltage (Ay and Zaidi, 2006a) on the accuracy of CTAC has been found to be relatively small. The latter reference above demonstrated that the use of a single calibration curve acquired under standard imaging conditions does not affect to a visible or measurable extent neurological PET images reconstructed using CTAC when CT images are acquired in different conditions (Ay and Zaidi, 2006a).

In a clinical setting, the use of CT images for attenuation correction of PET data can cause artefacts and may alter semi-quantitative measurements in some cases. Several investigators attempted to assess qualitatively and quantitatively the effect of physical and physiological parameters on the accuracy of CTAC in PET including misregistration of PET and CT images (Beyer et al., 2005), the administration of oral and intravenous contrast medium (Nakamoto et al., 2003; Nehmeh et al., 2003; Antoch et al., 2004; Ay and Zaidi, 2006b), the presence of metallic dental implants (Goerres et al., 2002; Kamel et al., 2003), respiratory motion (Osman et al., 2003) and truncation artefacts (Beyer et al., 2006) (in whole-body imaging), and X-ray scatter in CT images (Ay and Zaidi, 2006b). The latter effect is more pronounced in the next generation of flat panel detector-based cone-beam CT scanners, which are much less immune to scatter than fan-beam CT scanners (Siewerdsen et al., 2006). It has been shown that overcorrection of dense metallic dental implants and radiodense oral and intravenous contrast agents may cause hot-spot artefacts in the attenuation corrected PET images. As a rule of thumb, examination of the uncorrected images is recommended to distinguish technical artefacts from physiologic/pathologic hypermetabolism. Some investigators proposed to apply appropriate post-reconstruction correction procedures to reduce these artefacts.

Various methods for metal artefact reduction have been reported in the literature and used successfully in clinical and research settings (Wang et al., 2000; Zhao et al., 2000; De Man et al., 2000; Mahnken et al., 2003). On the other hand, one can account for attenuation differences between iodine/barium contrast versus bone by means of a technique that generates a calibration curve for contrast media, using a method similar to that employed for soft tissue and bone alone where separate calibration curves are generated for each material (e.g. iodine vs. bone) for different X-ray potentials used to acquire CT scans, and for different photon energies (Tang et al., 1999). Some investigators have proposed using image segmentation methods of converting CT numbers to

attenuation coefficients that correctly scale contrast enhanced CT images for intravenous (Tang et al., 1999) and oral (Carney et al., 2002) agents. In addition, other strategies including the acquisition of both pre-contrast and post-contrast CT scans can be utilized to minimize possible artefacts contributed by the presence of contrast media when the CT scan is to be used as an attenuation map for correction of the PET data (Townsend et al., 2004). More recently a segmented contrast correction (SCC) method was proposed by Nehmeh et al. (2003) to correct for oral contrast medium artefact in CTAC PET images. As an example, Fig. 7 shows typical attenuation maps and reconstructed PET images of an anthropomorphic striatal phantom (Radiology Support Devices Inc., Long Beach, CA) before and after correction using SCC algorithm referenced above using *a priori* knowledge of the presence of contrast medium (Ay and Zaidi, 2006b). The CT images of the RSD phantom were modified by inserting a 20 mm diameter cylindrical region in the main chamber to simulate the presence of positive contrast agents with various concentrations corresponding to CT number of 2000 HU.

The analysis of ACFs in the study referenced above for simulated cylindrical water phantom in both fan- and cone-beam CT scanners showed that the contamination of CT data with scattered radiation in the absence of scatter removal underestimates the true ACFs, namely by 7.3% and 28.2% in the centre for both geometries, respectively. The activity recovery coefficient (ARC) was 190.7% for a cylindrical volume of interest located in the main chamber of the striatal phantom containing contrast medium corresponding to 2000 HU, whereas the ARC was overestimated by less than 5% for the main chamber and ~2% for the left/right putamen and caudate nucleus compared to the absence of contrast medium.

Approaches requiring segmented MRI

The advent of image fusion techniques and dual-modality imaging systems has enabled new methods of quantifying uptake in PET data. A standard practice in many PET facilities is to define ROIs on a high-resolution T1-weighted MRI dataset to quantify radionuclide uptake in a coregistered multislice PET study. The ROIs are defined in the MRI image slices, and transformed to the coordinate space of the PET image. This technique allows to overcome spill-out effects and other errors related to the limited spatial resolution of the radionuclide image.

In addition to methods that use radionuclide or X-ray transmission sources to produce attenuation maps for reconstruction of PET data, a few studies have prospected the possibility of using segmented MRI data to construct an attenuation map for attenuation correction purposes in emission tomography. This approach is referred to here as MRI-guided attenuation correction (MGAC) and represents an outgrowth of the many PET/MR image coregistration and fusion algorithms that have been described in the literature (Hutton and Braun, 2003). The availability of public domain image registration and segmentation software dedicated for brain allows clinical implementation of MR-based attenuation correction. Likewise, the recent interest in simultaneous multi-modality PET/MRI (Marsden et al., 2002) may motivate future applications of this method to whole-body imaging where accurate software-based registration is more difficult to achieve. While the advantages of combined PET/CT could in principle be replicated by combined PET/MRI, the clinical usefulness of simultaneous PET/MRI in whole-body PET imaging is not yet established. In addition, there are still several important challenges that must be overcome in implementing and operating a combined PET/MRI imaging system (Townsend and Cherry, 2001).

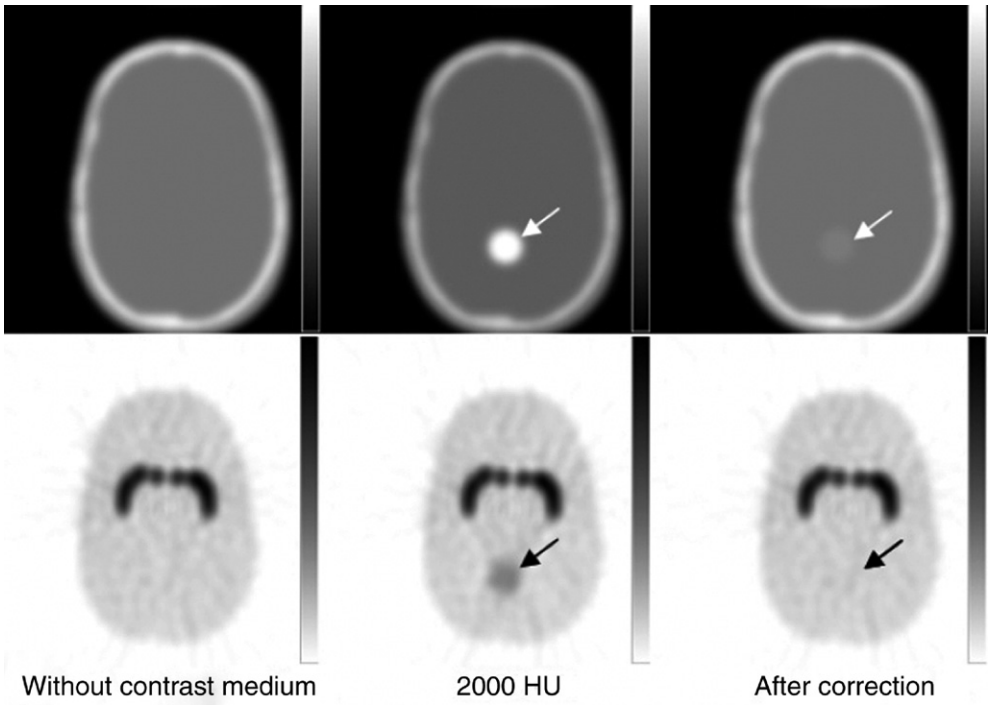

Fig. 7. Representative slice of the CT-based attenuation map (top) and reconstructed emission PET image (bottom) of the anthropomorphic striatal phantom modified by inserting a cylindrical area containing given concentration of contrast medium corresponding to 2000 HU. From left to right: absence of contrast medium, presence of contrast medium without correction and after applying the segmented contrast correction (SCC) algorithm to the circular region concentrating contrast medium. Reprinted with permission from Ay and Zaidi (2006b).

In comparison to X-ray CT, MRI typically is more expensive, involves longer scan times, and produces anatomical images from which it is more difficult to derive attenuation maps for correction of the PET emission data (Hasegawa and Zaidi, 2005). Moreover, virtually all clinical PET imaging detector blocks use photomultiplier tubes whose performance can be seriously affected in the presence of magnetic fields which are significantly smaller than those produced by modern MRI scanners. This is especially problematic in an MRI scanner which relies on rapidly switching gradient magnetic fields and radiofrequency (RF) signals to produce the magnetic resonance image. The presence of the magnetic field gradients and RF signals certainly could disrupt the performance of a photomultiplier tube and PET detector if they were located within or adjacent to the magnet of the MRI system. Similarly, the operation of the MRI system relies on a very uniform and stable magnetic field to produce the MR image. The introduction of radiation detectors, electronics, and other bulk materials can perturb the magnetic field in a way that introduces artefacts in the MR image.

For imaging the brain, the simplest method segments the MRI image by thresholding to create a mask, which delineates the skull and all other tissues but excludes the hollow space of sinus, etc. Every voxel in the mask is then assigned the attenuation coefficient of water (e.g. 0.096 cm^{-1} for 511 keV). In the approach adopted by El Fakhri et al. (2003) for SPECT, the MRI is segmented into bone and soft tissue classes to yield a nonuniform attenuation map by modifying the uniform attenuation map to model bone of the skull by the water thickness that would result in the same attenuation (e.g. μ=0.153 cm^{-1} at 140 keV). A nonuniform water envelope is then added to the surface of the brain to account for nonuniform bone compartment.

A more robust approach based on registered 3-D MRI T1 images has been proposed recently (Zaidi et al., 2003). These images were realigned to preliminary reconstructions of PET data and then segmented using a fuzzy clustering technique by identifying tissues of significantly different density and composition. The voxels belonging to different regions can be classified into bone, brain tissue and sinus cavities. These voxels were then assigned theoretical tissue-dependent attenuation coefficients as reported in the ICRU 44 report (ICRU, 1989). One of the limitations of this method is that the difficulties associated with automatic segmentation of the skull on the T1-weighted spin-echo images using the fuzzy clustering algorithm led to some manual intervention of the operator. This consists of filling the complex shaped skull base using a morphological "closing" operation to make it more uniform. Multispectral MR data acquisition with varying contrast characteristics including spin-echo T2-weighted and proton spin density (PD)-weighted sequences provides additional information for distinguishing between different tissues and could be an interesting approach to solve this problem. Careful optimisation of the MR sequences is a prerequisite for successful implementation of the technique and needs to be investigated further. Another appealing approach would be to explore new techniques for segmentation of skull in human T1-weighted MRI using a sequence of mathematical morphological operations (Dogdas et al., 2005). Prior to the segmentation of skull, the algorithm segments the scalp and the brain from the MR image. The scalp mask allows to quickly eliminate background voxels with intensities similar to those of the skull, while the brain mask ensures that the brain does not intersect the skull segmentation. The inner and the outer skull boundaries can be computed using thresholding and morphological closing and opening operations. The results are then masked with the scalp and brain volumes to guarantee closed and nonintersecting skull boundaries. Fig. 8 illustrates the performance of MRI-guided derivation of the attenuation map as compared to the CT-based approach for clinical brain PET imaging. The figure shows the transaxial CT cross-section, the corresponding coregistered MRI cross-section and the segmented MRI required to generate a three tissue compartment head model corresponding to brain, skull and scalp using the algorithm mentioned above (Dogdas et al., 2005). Compensation for attenuation in the bed and head holder can be accomplished as discussed above for calculated attenuation correction methods.

Attenuation correction strategies in brain PET studies

The fundamental equation that links the imaged object $f(x,y)$ and corresponding attenuation map $\mu(x,y)$ to its measured projections $p(s,\phi)$ is called the attenuated Radon transform and is given in the case of PET by:

$$p(s,\phi) = \int_{L(s,\phi)} f(x,y)\mathrm{d}r \times \exp\left[-\int_{L(s,\phi)} \mu(x,y)\mathrm{d}l\right]\mathrm{d}r \qquad (5)$$

where $L(s,\phi)$ is as defined in Eq. (3) above and ϕ is the angle between the rotating detector plane and the stationary reconstruction plane.

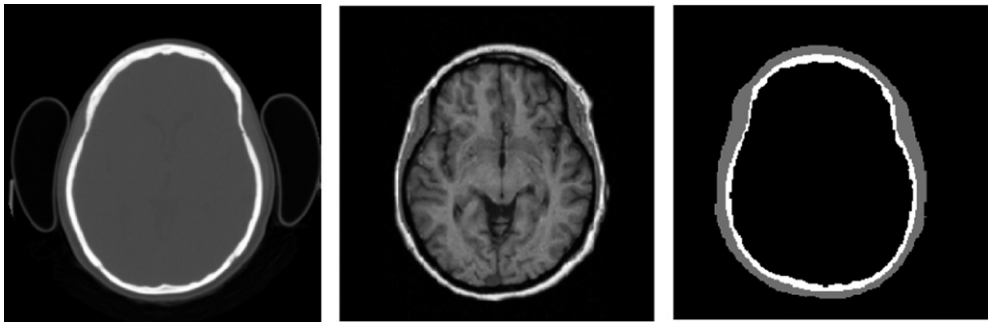

Fig. 8. Illustration of the performance of MRI-guided derivation of the attenuation map as compared to CT-based approach for clinical brain PET imaging. From left to right: transaxial CT cross-section section and its corresponding coregistered MRI cross-section and the segmented MRI required to generate a three tissue compartment head model corresponding to brain, skull and scalp. White voxels are labelled as skull, dark grey voxels are labelled as scalp, and intracranial black voxels are labelled as brain tissue.

The ideal solution would have been to use an exact solution for the inverse problem to solve the Radon transform and reconstruct the spatial distribution of the tracer $f(x,y)$. However, owing to the complexity of the equation in the case of nonuniform attenuation, an exact solution is not possible in general. The seminal contribution by Novikov (2002) who recently gave an explicit inversion formula for the attenuated Radon transform for a particular important family of weights was a major breakthrough in the field. Moreover, Novikov's formula was proven for a somewhat larger class of weight functions using a completely different and more straightforward method (Natterer, 2001; Boman and Stromberg, 2004). In spite of recent progress, various approximate methods have been proposed and are still used to solve the problem of reconstructing an object from its measured projections in the presence of photon attenuation.

Measured transmission scanning for attenuation correction purposes was used during the early developments of PET, which started mainly as a research tool with greater emphasis on accurate quantitative analysis. Two additional factors contributed to this logical advancement: first, attenuation correction in PET is relatively straightforward since in principle it requires a simple pre-multiplication of the measured emission data by the corresponding ACFs, and second, the ACFs in PET are large and without attenuation compensation, quantification is unable to be realized.

As mentioned previously in the Magnitude of attenuation section, photon attenuation in PET is independent of the emission point along this LOR. In contrast, modelling the attenuation process in SPECT involves taking into account the fact that attenuation factors are dependent on the emission point since the emitted photon crosses only part of the patient's anatomy before reaching the detector. The direct consequence is that nonuniform attenuation correction for SPECT generally requires iterative reconstruction.

Because attenuation correction in PET is relatively straightforward and its accuracy is limited only by the noise (statistics) present in the acquired transmission scans, only two techniques have materialized and both require the computation of the ACFs through forward projection of the attenuation map at appropriate angles. To reduce processing time and data storage requirements for 3-D PET data collection mode, it is often convenient to work with pre-corrected data. This is the basis of the first approach where data correction is carried out in projection space through multiplication of the ACFs by the measured emission data using the following expression:

$$p_{\mathrm{AC}}(s,\phi) = \mathrm{ACF} \times p(s,\phi) = \int_{L(s,\phi)} f(x,y)\mathrm{d}r \tag{6}$$

The attenuation corrected projections are then used to reconstruct the images using either analytic or iterative reconstruction techniques. An attractive option is to produce a smaller set of sinograms by pre-correcting the data and applying Fourier rebinning (FORE). However, the data are no longer Poisson distributed. It has been shown that iterative algorithms (e.g. Ordered Subsets–Expectation Maximisation or OS–EM) yield suboptimal images from such data (Comtat et al., 1998). Alternatively, when OS–EM is used, the ACFs can be applied to provide proper statistical weighting to the data as is done in attenuation-weighted OS–EM (AWOSEM) (Comtat et al., 1998). This latter technique has better noise properties and is now part of commercial software used routinely in many clinical PET facilities. For instance, it has been shown that the FORE+AWOSEM algorithm results in the best overall detection and localization performance for 1-cm-diameter lesions compared with FORE+OSEM and FORE+FBP algorithms in PET imaging (Lartizien et al., 2003).

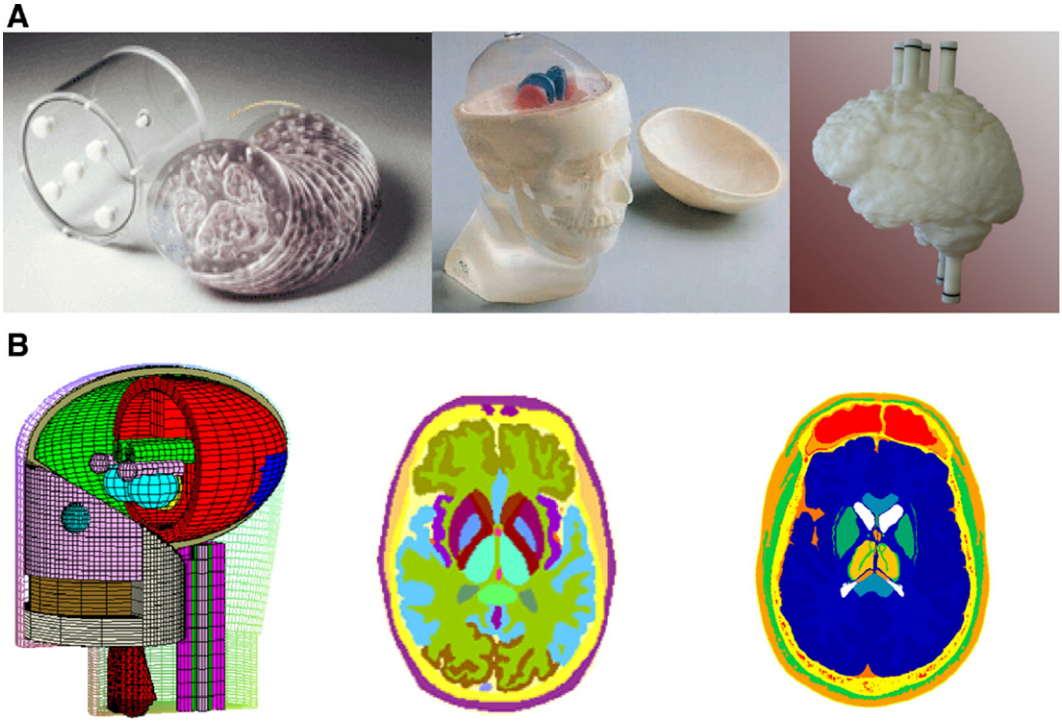

Fig. 9. Illustration of anthropomorphic physical (A) and software (B) brain phantoms used for development and evaluation of attenuation correction methodologies in PET (Photographs courtesy of Data Spectrum Corporation, USA, Radiology Support Devices Inc., USA, and Dr B. Alfano, Napoli, Italy, respectively). Software phantoms shown are kindly supplied by their developers (Bouchet and Bolch, 1999; Zubal et al., 1994; Chao and Xu, 2004).

Evaluation of attenuation correction approaches

Before attenuation correction procedures can be trusted, the model and its computerized implementation must be validated. Most of the attenuation correction algorithms developed so far have been evaluated using either simulated or experimentally measured phantom studies, in addition to qualitative and/or quantitative evaluation of clinical data. This has been extended more recently to objective assessment of image quality using Receiver Operating Characteristics (ROC) analysis based on human or computer observers (Hustinx et al., 2000), evaluation of the influence of attenuation correction techniques on tracer kinetic parameter estimation (Sossi et al., 2005) and voxel-based analysis in functional brain imaging using statistical parametric mapping (Mesina et al., 2003). However, the absence of a *gold standard* when dealing with clinical data complicates the evaluation procedure. Further research and development efforts are clearly needed to establish standardized and worldwide-accepted validation strategies and guidelines.

Availability of software and experimental phantoms

The availability in the public domain and dissemination of well characterised experimental and simulated data sets between research groups represent an important step for fast and objective evaluation of image correction procedures. The advantage of using phantom studies is that the ground truth is known *a priori*. PET simulation tools have been shown to be very useful for validation and comparative evaluation of attenuation correction techniques, since it is possible to obtain a reference image to which reconstructed images should be compared (Zaidi, 1999). One such Monte Carlo simulated database, including PET EM and TX data providing the imaging community with realistic simulated 3-D and 4-D (including

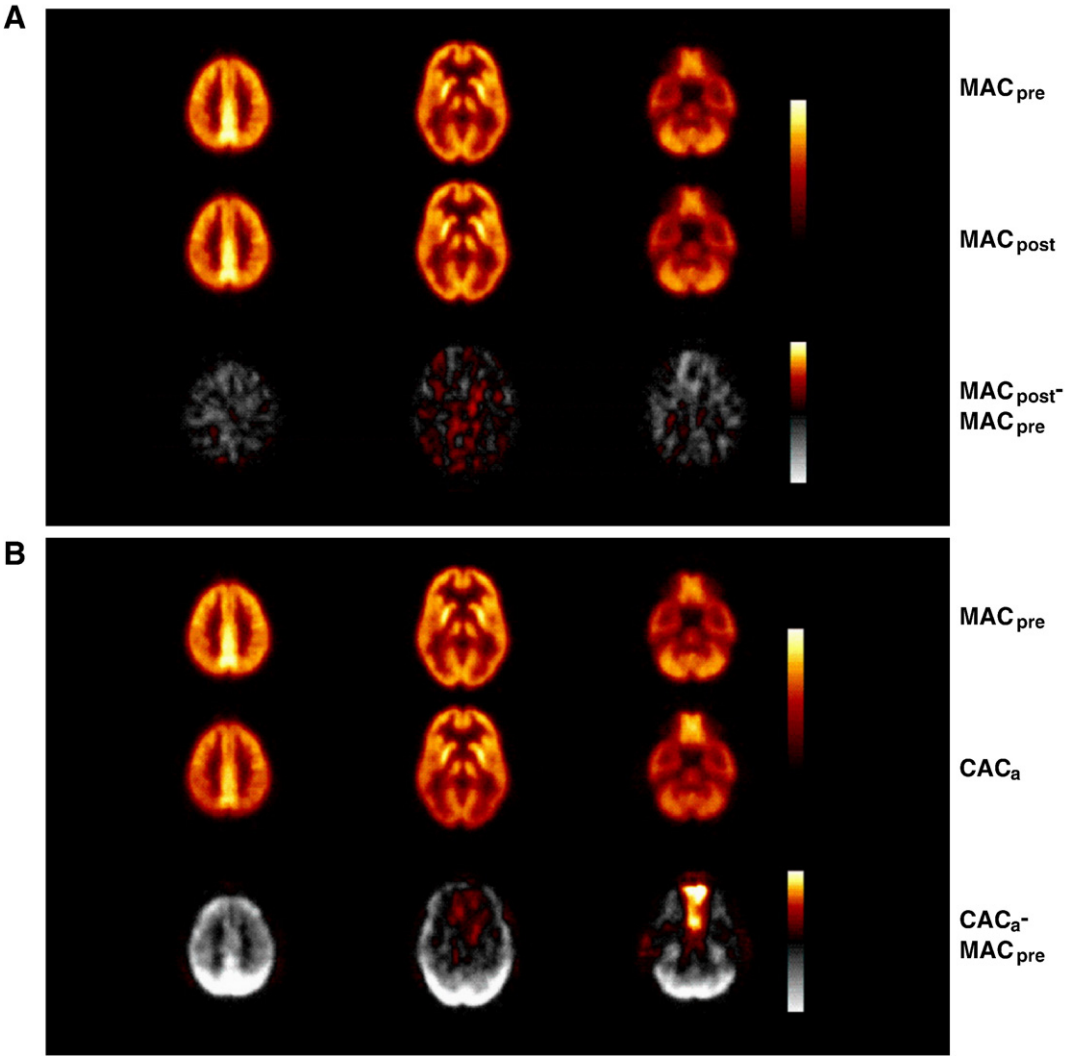

Fig. 10. (A) Average and subtraction images comparing post-injection transmission using simultaneously acquired emission data for subtraction (MAC_{set}) with pre-injection transmission scanning (MAC_{pre}). (B) Average and subtraction images comparing automated calculated attenuation correction (CAC_a) with MAC_{pre}. For each panel, average images obtained by MAC_{pre} are shown in top row; method being compared is shown in middle row and difference images are shown in bottom row. Colour scale for bottom row is split to indicate positive differences in "hot-iron" scale and negative differences in grey scale. Difference images are windowed to a maximum absolute difference of 10%. Reprinted with permission from Hooper et al. (1996).

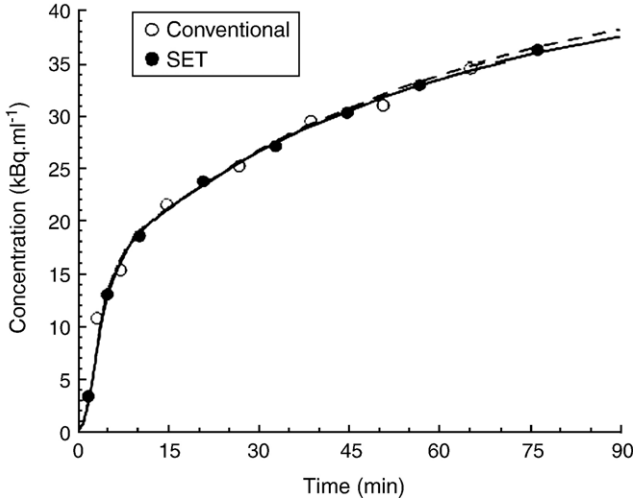

Fig. 11. Time–activity curves for grey matter of a patient obtained using two attenuation correction methods. Data points corresponding to conventional pre-injection transmission scanning image frames are indicated by open circles (model fit shown as solid line) and those corresponding to simultaneous emission and transmission (SET) frames are indicated by filled circles (model fit shown as dashed line). Reprinted with permission from Meikle et al. (1997).

time information) PET studies for commonly used radiotracers, is available for academic use (Reilhac et al., 2005).

The popularity of simulations stimulated the development of computational models of the human anatomy and dedicated simulation tools. Computerized phantoms can either be defined by mathematical (analytical) functions or digital (voxel-based) volume arrays. For instance, the MIRD Committee in his Pamphlet No. 15 (Bouchet et al., 1999) adopted 6 age-specific mathematical models of the head and brain representing average reference brain and head for a newborn, 1-year-old, 5-year-old, 10-year-old, 15-year-old (also representing the average adult female), and adult male (Bouchet and Bolch, 1999). Although these phantoms were intended to provide better dosimetric tools for functional neuroimaging, they might be useful for assessing attenuation correction techniques in paediatric neuroimaging procedures for example.

More realistic modelling is best achieved with phantom models that match the gross parameters of an individual patient. Anthropomorphic phantoms with internally segmented structures make clinically realistic simulations possible. A typical high resolution anthropomorphic voxel-based brain phantom was developed by Zubal et al. (1994) using on an MRI brain scan of a human volunteer, manually segmented by medical experts. Alternatively, the group at Montreal Neurological Institute (MNI, Canada) developed a low-noise brain model by averaging several scans of a single subject in stereotaxic space (Collins et al., 1998). This brain phantom proved to be suitable for MRI (Kwan et al., 1999) and PET simulations (Ma et al., 1993). More recently, a new voxel-based whole body model, called VIP-Man (Xu et al., 2000), and a head/brain model (Chao and Xu, 2004) have been developed using high resolution transversal colour photographic images obtained from the National Library of Medicine's VH Project (Spitzer and Whitlock, 1998).

Physical phantoms of various degree of complexity can be used to demonstrate the performance or limitation of a specific attenuation correction procedure. They include simple geometrical objects or structures with uniform or ideally nonuniform attenuation properties. Validation is usually sought out by first making sure the attenuation correction method works well compared to well established methods used in clinical settings. For example, the uniform Hoffman 3-D brain phantom (Hoffman et al., 1990) was used for characterisation of many algorithms (Van Laere et al., 2000; Montandon et al., 2003). A more thorough experimental setup enabling data acquisition with negligible degrading effects from scatter and attenuation was also proposed (Larsson et al., 2000). It consists of using a subresolution stacked "sandwich" slice design constructed using a high-resolution digital phantom. The principle is based on discrete sampling of radioactivity in 3-D objects by means of subresolution-spaced equidistant 2-D planes, on which *a priori*-defined radioactivity distributions are printed on paper sheets using radioactive ink. This design theoretically allows for scatter and attenuation free imaging when air is used and realistic imaging conditions with appropriate photon scattering and attenuation losses when a dense material (e.g. polystyrene plates) is used between the 2-D planes. The technique allows one to obtain "ideal" experimental images (resulting essentially from primary photons) for comparison with "real" images degraded by photon scattering and attenuation.

Assessment studies are further carried out with phantoms of increased complexity, having different compartments including different brain structures and a bone like structure representing the skull. Realistic phantoms containing several independent compartments surrounded by a realistic medium, such as the brain phantom used to validate the geometric transfer matrix (GTM)-based partial volume correction approach (Rousset et al., 1998) or the commercial anthropomorphic striatal phantom (Radiology Support Devices Inc., Long Beach, CA) used to assess sources of error and artefact in CTAC (Ay and Zaidi, 2006a, 2006b) represent more realistic imaging conditions. Those models are suitable for neuroreceptor studies where the tracer accumulates specifically in the striatum. For tracers diffusing more homogeneously throughout the cortex, an anthropomorphic phantom (STEPBRAIN) separating the cortex

Table 2
^{18}F-FDG model parameter estimates from simultaneous emission and transmission (MAC_{set}) and conventional pre-injection transmission scanning (MAC_{pre}) imaging in patient study

	Grey matter			White matter			Tumour		
	MAC_{pre}	MAC_{set}	Bias (%)	MAC_{pre}	MAC_{set}	Bias (%)	MAC_{pre}	MAC_{set}	Bias (%)
K_1	0.102±0.006	0.108±0.006	+6	0.041±0.002	0.046±0.006	+12	0.114±0.003	0.09±0.01	−21
k_2	0.18±0.04	0.19±0.03	+6	0.09±0.02	0.11±0.04	+22	0.21±0.01	0.14±0.04	−33
k_3	0.07±0.02	0.07±0.01	0	0.039±0.007	0.05±0.02	+28	0.031±0.002	0.029±0.007	−6
k_4	0.007±0.005	0.006±0.002	−14	–	–	–	–	–	–
lCMRGlu	6.0±0.6	5.9±0.4	−2	2.7±0.2	2.9±0.3	+7	3.2±0.1	3.2±0.3	0

Reprinted with permission from Meikle et al. (1997).

from white matter has been recently proposed (Alfano et al., 2003). Fig. 9 illustrates examples of physical and software phantoms widely used for development and evaluation of attenuation correction techniques in brain PET. Software and experimental head/brain phantoms are generally limited in terms of their applicability due to the limitation in complexity one can achieve in reproducing the human head and brain. However, physical phantom experiments are mostly used for validation purposes and represent the *sine qua non* step for proper acceptance of a particular algorithm.

Comparison of methods involving clinical and research studies

The application of attenuation correction in clinical setting requires a rigorous assessment in order to define the most appropriate algorithm for a specific application and give an estimate of expected accuracy. However, evaluation of attenuation correction and other image processing techniques in a clinical environment is hampered by the multiplicity of the medical purposes for which the corrections may be studied. Furthermore, investigators must be eager to compare clinical results with and without attenuation

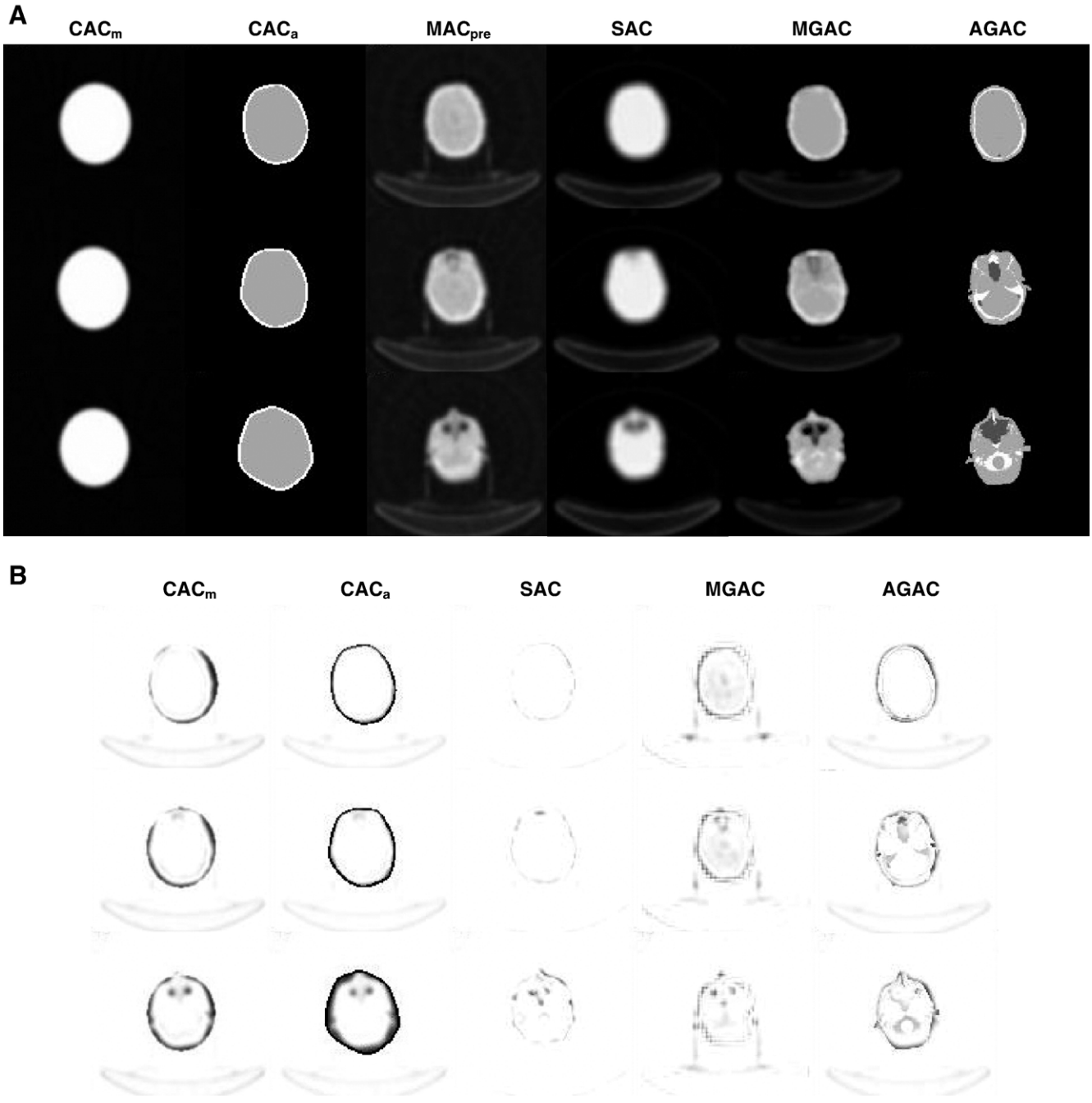

Fig. 12. (A) Three different transaxial planes of a patient study illustrating attenuation maps derived using different methods. From top to bottom: superior, middle and inferior planes and from left to right: CAC_m, CAC_a, MAC_{pre}, SAC, MGAC, and finally AGAC. (B) Difference of images shown in panel A obtained by subtracting transmission-based (MAC_{pre}) attenuation map planes from attenuation map planes derived using alternative techniques. From left to right: CAC_m, CAC_a, SAC, MGAC, and finally AGAC. Adapted with permission from Zaidi et al. (2004).

correction, which in most cases doubles the work, rather than simply choosing to use attenuation correction or not to use it (Wahl, 1999). It should be stressed that the requirements for clinical and research studies are different, the latter requiring greater emphasis on quantitative accuracy.

The widely accepted gold standard is transmission-based measured attenuation correction performed prior to administration of the radiopharmaceutical to the subject. However, it is an imperfect gold standard due to the presence of noise in the measurement, as discussed above, and it is not always practical. Therefore, a wide variety of alternative approaches are routinely employed to minimise the time required for the transmission measurement or eliminate it altogether. Each of the approaches discussed so far has advantages and disadvantages, but only a detailed clinical evaluation can reveal their relative performance and impacts on accuracy and image quality.

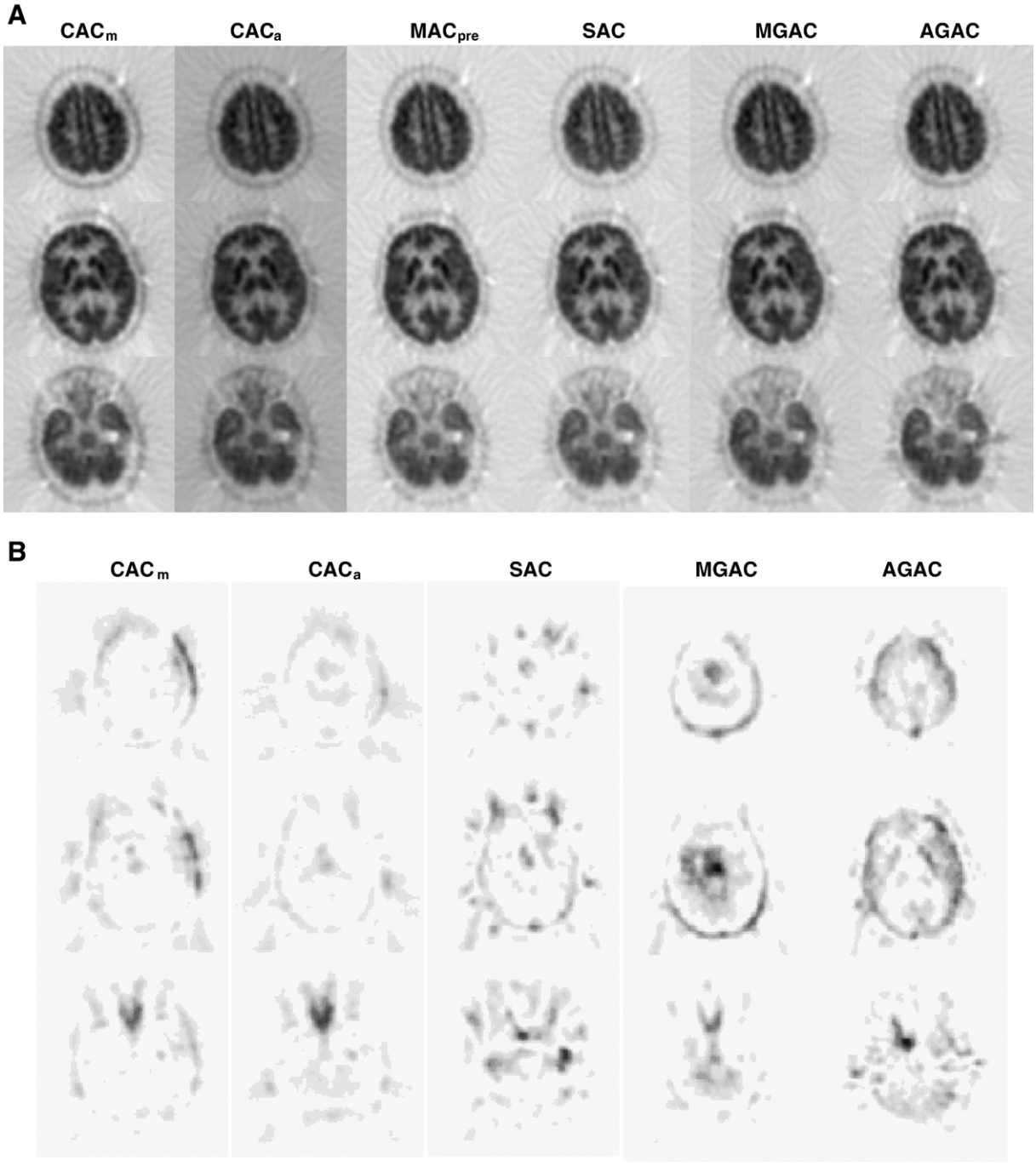

Fig. 13. (A) Three different transaxial PET images of a patient study reconstructed using different attenuation correction techniques. From top to bottom: superior, middle and inferior planes and from left to right: CAC_m, CAC_a, MAC_{pre}, SAC, MGAC, and finally AGAC. (B) Difference of images shown in panel A obtained by subtracting reconstructions guided by measured transmission (MAC_{pre}) from reconstructions guided by alternative attenuation correction techniques. From left to right: CAC_m, CAC_a, SAC, MGAC, and finally AGAC. Adapted with permission from Zaidi et al. (2004).

Hooper et al. (1996) performed a study comparing three methods of attenuation correction for neurological PET studies: transmission-based pre-injection scanning (MAC_{pre}), post-injection transmission scanning (MAC_{post}), and automated calculated attenuation correction (CAC_a). Two post-injection methods were employed: one that estimates the emission contamination of the post-injection scan using a short transmission "mock" scan performed after tracer administration, and one that estimates the emission contribution directly from the simultaneously recorded EM and TX measurements (MAC_{set}). A cohort of 26 patients undergoing routine FDG-PET imaging for various neurological conditions was included in the study. After performing attenuation correction with each of these methods, images were reconstructed and then transformed to a standard stereotaxic space using a computerised brain atlas (Greitz et al., 1991) for quantitative comparison of local cerebral metabolic rate of glucose (LCMRGlu) values. The key findings of this study were:

1. Excellent agreement was observed between LCMRGlu values derived from post-injection TX measurements and those derived from pre-injection TX data;
2. Calculated attenuation correction gave rise to significant bias in several brain regions. Most notably, it underestimates LCMRGlu by up to 23% in areas where brain tissue is in close proximity to thick skull bones (e.g. occipital association cortex and cerebellum) and overestimates LCMRGlu by up to 12% where brain tissue is in close proximity to the sinus cavities (e.g. gyrus recti).
3. Post-injection transmission scanning markedly reduces study duration (by eliminating the delay between TX and EM scans) without loss of quantitative accuracy.

Fig. 10 illustrates the close agreement between pre-injection and post-injection transmission scanning methods and the bias introduced by calculated attenuation correction. The magnitude of the bias was fully appreciated in earlier studies published in the 1980s (Huang et al., 1979; Lammertsma et al., 1982). Using similar study design, some investigators came to conclusions not as transparently justified to the authors of this review as the ones presented above (Setani et al., 2000).

A follow-up study investigated the utility of simultaneous EM and TX scanning during dynamic neurological PET studies (Meikle et al., 1997). Dynamic scanning is not normally performed in clinical studies but, in conjunction with frequent arterial blood sampling, it is the method of choice when accurate estimates of LCMRGlu or receptor binding parameters are required. In this study, a patient with a brain tumour underwent dynamic FDG-PET scanning with interleaved emission only and emission plus transmission frames throughout the 80 min scan. A pre-injection transmission scan was also performed and used to correct the emission only frames for attenuation using conventional methodology. LCMRGlu was estimated separately for the simultaneous and emission only data in each of three brain regions (including the tumour) using the standard 3 compartment FDG model (Sokoloff et al., 1977; Phelps et al., 1979) and non-linear least squares model fitting. The time–activity curves and model fit derived from the normal grey matter region are shown in Fig. 11. The bias in LCMRGlu values derived from the simultaneous data was less than 10% compared with the values obtained using conventional methodology. In addition, parameter estimates calculated for gray matter, white matter, and tumour ROIs in each acquisition mode are given in Table 2. It should be noted that there was very good agreement between MAC_{set} and conventional MAC_{pre} imaging for estimating LCMRGlu in all three ROIs. The agreement between the two methods was also good for estimating individual rate constants in gray matter, but was not as good for white matter and tumour data, which were relatively more noisy. This is also evident in the increased uncertainty in estimating the rate constants in these regions.

Thus, transmission scans performed following radiopharmaceutical administration are feasible and introduce minimal bias in clinical and research neurological FDG PET studies, with the advantage of reduced study time and less likelihood of patient movement between the TX and EM scans. To the best of our knowledge, except the work by Lammertsma et al. (1982) for ^{15}O-labeled tracers, studies comparing measured and calculated attenuation correction have not been performed for radiopharmaceuticals other than FDG but it seems reasonable to extrapolate the results of these studies to other tracers, including receptor binding radioligands. The bias introduced by calculated attenuation correction demonstrated by Hooper et al. (1996) is particularly relevant to receptor binding studies, where the cerebellum is frequently used to derive a reference tissue curve as an input function in receptor binding models (Lammertsma and Hume, 1996; Gunn et al., 1997).

The quantitative accuracy of the segmented MAC_{post}-based attenuation correction technique was further evaluated more recently using clinical data acquired in both 2D and 3-D modes (Kaneko et al., 2004). It was reported that there is good correlation between activity concentration values obtained by this technique and those obtained by the pre-injection transmission technique using ROI-based analysis whereas no significant differences between the two techniques were observed using the voxel-based analysis by means of SPM.

In a more thorough comparative assessment study, Zaidi et al. (2004) compared the impact of the attenuation map on absolute and relative quantification using clinical brain scans corrected for attenuation using both uniform attenuation maps based on manual (CAC_m) and automatic (CAC_a) contours and nonuniform attenuation maps described above. The latter class of algorithms include conventional pre-injection transmission scanning (MAC_{pre}) (Zaidi et al., 2001), segmented transmission (SAC) (Xu et al., 1996), coregistered segmented MRI (MGAC) (Zaidi et al., 2003), and the Atlas-guided method (AGAC) (Stodilka et al., 2000). This later method was implemented as described by Stodilka et al. without any alteration (e.g. adding the bed to the final images). Several image quality parameters were compared including the mean squared error between the different attenuation maps and absolute and relative quantification indexes for PET images and correlation between them checked (Montandon, 2005). From a purely qualitative analysis, the merits of the more exact methods based on realistic nonuniform attenuation maps are obvious. They produce less visible artefacts, while the approximate methods (CAC_a) tend to produce an artefact in which there is a high level of activity along the edge of the image due to overestimation of the head contour on the external slices when using the automatic edge detection method. On the other hand, the quantitative VOI-based analysis of 10 patient data sets revealed different performance and statistically significant differences between the different attenuation correction techniques when compared to the gold standard (MAC_{pre}).

Representative planes (superior, middle and inferior) of attenuation maps generated using the different methods for a clinical brain

PET study with difference images calculated by subtracting MAC_{pre}-based from alternative methods for deriving the attenuation map are shown in Fig. 12. It is worth noting the slight rotational misregistration between the TX and EM scans for this patient. In fact, the misalignment between EM and TX scans is reflected by a clearly visible rotational misregistration between MAC_{pre} and CAC_a attenuation maps, the latter being computed from the emission scan. This misalignment is well recovered by both MGAC and AGAC procedures. The MRI-PET co-registration algorithm seems to produce smaller errors compared to TX-EM even when thermoplastic face mask is used for reproducible patient positioning. Non-uniformities of the attenuation map are obvious on planes containing sinus and air cavities. The mean squared error between the different attenuation maps is also larger when using this latter method owing to the fact that the current implementation of this method significantly overestimates the head contours on the external slices.

Corresponding reconstructed PET emission images and difference images obtained by subtracting reconstructions guided by MAC_{pre} from reconstructions guided by alternative attenuation correction techniques are illustrated in Fig. 13. The qualitative evaluation showed no significant differences between the different attenuation correction techniques as assessed by expert physicians except CAC_a, which generates artefacts in the upper edges of the head. Correlation in mean regional cerebral glucose metabolism (rCGM) values with respect to the gold standard (MAC_{pre}) was good, except for CAC_a ($R^2=0.54$). The SAC and MGAC methods showed the best correlation ($R^2=0.90$) and the regression lines agreed well with the line of identity. Relative differences in mean rCGM values were in general less than 8%. Nevertheless, ANOVA results showed statistically significant differences between the different methods for some regions of the brain (Zaidi et al., 2004).

Summary and future directions

High resolution cutting-edge PET neuroimaging is poised to advance our understanding of the pathophysiological mechanisms of neurological and psychiatric diseases and in the clinical management of patients. Frontiers of molecular imaging research are also being expanded with small animal imaging of the brain with dedicated high resolution PET instrumentation in addition to optical imaging and high-field MR imaging. The capability to accurately perform attenuation correction with validated commercial hardware/software solutions by use of strict quality-control measures enhances the interpretive confidence and accuracy of functional brain PET imaging. As a result, there has been growing clinical acceptance of attenuation correction by clinicians and practitioners. Pre-injection transmission scanning remains the most widely used method, although this is rapidly changing with the advent of dual-modality scanners, especially PET/CT scanners. Automated implementations of MRI-guided attenuation correction (Zaidi et al., 2003) using more sophisticated coregistration and segmentation strategies remains a promising approach and might be the method of choice for the foreseeable future of dedicated brain PET units not equipped with transmission scanning units (Braem et al., 2004; Seguinot et al., 2006).

The development of transmissionless attenuation correction methodologies remains an active research area. Some of these methods are considerably more computationally intensive than conventional techniques especially for large aperture cameras with fine sampling (Krol et al., 2001). The most promising approaches belonging to this class of techniques use either continuous (Natterer, 1993; Welch et al., 1998, 2003; Bromiley et al., 2001) or discrete (Bronnikov, 1999, 2000) consistency conditions. It has recently been shown that the discrete consistency conditions can be used to estimate the thresholds for segmentation of the transmission image (Welch et al., 2003) and to assess regularization parameters for attenuation map reconstruction (Panin et al., 2004). It should be emphasized that the clinical applicability of these approaches still remains to be confirmed.

Noticeable progress in attenuation compensation has been made in the last decade, the main opportunities arising from the availability of both improved hardware design configurations for transmission scanning and innovative and faster image processing algorithms. This has permitted the implementation of much more ambitious algorithms that tackle not just brain imaging but the full range of whole-body imaging using PET.

Acknowledgments

This work was supported by the Swiss National Science Foundation under grant SNSF 3152A0-102143 and the Research and Development Foundation of Geneva University Hospital under grant PRD-04-1-08.

References

Alenius, S., Ruotsalainen, U., Astola, J., 1999. Attenuation correction for PET using count-limited transmission images reconstructed with median root prior. IEEE Trans. Nucl. Sci. 46, 646–651.

Alfano, B., Brunetti, A., Prinster, A., Quarantelli, M., Salvatore, M., 2003. "STEPBRAIN: a stereolithographed phantom of the brain for nuclear medicine: computed tomography, and magnetic resonance applications. (abstract)". Annual meeting of the Radiological Society of North America, Chicago, USA.

Anderson, J.M.M., Srinivasan, R., Mair, B.A., Votaw, J., 2002. Hidden Markov model based attenuation correction for positron emission tomography. IEEE Trans. Nucl. Sci. 49, 2103–2111.

Antoch, G., Freudenberg, L.S., Beyer, T., Bockisch, A., Debatin, J.F., 2004. To enhance or not to enhance? 18F-FDG and CT contrast agents in dual-modality 18F-FDG PET/CT. J. Nucl. Med. 45 (Suppl. 1), 56S–65S.

Arlig, A., Gustafsson, A., Jacobsson, L., Ljungberg, M., Wikkelso, C., 2000. Attenuation correction in quantitative SPECT of cerebral blood flow: a Monte Carlo study. Phys. Med. Biol. 45, 3847–3859.

Ay, M.R., Zaidi, H., 2006a. Computed Tomography-based attenuation correction in neurological positron emission tomography: evaluation of the effect of X-ray tube voltage on quantitative analysis. Nucl. Med. Commun. 27, 339–346.

Ay, M.R., Zaidi, H., 2006b. Assessment of errors caused by X-ray scatter and use of contrast medium when using CT-based attenuation correction in PET. Eur. J. Nucl. Med. Mol. Imaging 33, 1301–1313.

Ay, M., Zaidi, H., in press. Impact of X-ray tube settings and metallic leads on neurological PET imaging when using CT-based attenuation correction. Nucl Instr Meth A.

Bai, C., Kinahan, P.E., Brasse, D., Comtat, C., Townsend, D.W., et al., 2003a. An analytic study of the effects of attenuation on tumor detection in whole-body PET oncology imaging. J. Nucl. Med. 44, 1855–1861.

Bai, C., Shao, L., Da Silva, A.J., Zhao, Z., 2003b. A generalized model for the conversion from CT numbers to linear attenuation coefficients. IEEE Trans. Nucl. Sci. 50, 1510–1515.

Bailey, D.L., 1998. Transmission scanning in emission tomography. Eur. J. Nucl. Med. 25, 774–787.

Berger, M.J., Hubbell, J.H., Seltzer, S.M., Chang, J., Coursey, J.S., et al., 1998 (http://physics.nist.gov/PhysRefData/Xcom/Text/XCOM.html).

Bergstrom, M., Litton, J., Eriksson, L., Bohm, C., Blomqvist, G., 1982.

Determination of object contour from projections for attenuation correction in cranial positron emission tomography. J. Comput. Assist. Tomogr. 6, 365–372.
Bettinardi, V., Gilardi, M.C., Cargnel, S., Rizzo, G., Teras, M., et al., 1994. A hybrid method of attenuation correction for positron emission tomography brain studies. Eur. J. Nucl. Med. 21, 1279–1284.
Bettinardi, V., Pagani, E., Gilardi, M., Landoni, C., Riddell, C., et al., 1999. An automatic classification technique for attenuation correction in positron emission tomography. Eur. J. Nucl. Med. 26, 447–458.
Beyer, T., Kinaham, P.E., Townsend, D.W., Sashin, D., 1994. The use of X-ray CT for attenuation correction of PET data. Proc. IEEE Nuclear Science Symposium and Medical Imaging Conference, 30 Oct.–5 Nov. Trendler RC, Norfolk, VA, USA, pp. 1573–1577.
Beyer, T., Tellmann, L., Nickel, I., Pietrzyk, U., 2005. On the use of positioning aids to reduce misregistration in the head and neck in whole-body PET/CT studies. J. Nucl. Med. 46, 596–602.
Beyer, T., Bockisch, A., Kuhl, H., Martinez, M.J., 2006. Whole-body 18F-FDG PET/CT in the presence of truncation artifacts. J. Nucl. Med. 47, 91–99.
Bilger, K., Kupferschlager, J., Muller-Schauenburg, W., Nusslin, F., Bares, R., 2001. Threshold calculation for segmented attenuation correction in PET with histogram fitting. IEEE Trans. Nucl. Sci. 48, 43–50.
Blankespoor, S.C., Xu, X., Kaiki, K., Brown, J.K., Tang, H.R., et al., 1996. Attenuation correction of SPECT using X-ray CT on an emission–transmission CT system: myocardial perfusion assessment. IEEE Trans. Nucl. Sci. 43, 2263–2274.
Bloomfield, P.M., Spinks, T.J., Reed, J., Schnorr, L., Westrip, A.M., et al., 2003. The design and implementation of a motion correction scheme for neurological PET. Phys. Med. Biol. 48, 959–978.
Boman, J., Stromberg, J.-O., 2004. Novikov's inversion formula for the Attenuated Radon Transform—A new approach. J. Geom. Anal. 14, 185–198.
Bouchet, L.G., Bolch, W.E., 1999. Five pediatric head and brain mathematical models for use in internal dosimetry. J. Nucl. Med. 40, 1327–1336.
Bouchet, L.G., Bolch, W.E., Weber, D.A., Atkins, H.L., Poston, J.W., 1999. MIRD pamphlet no. 15: radionuclide *S* values in a revised dosimetric model of the adult head and brain. Medical internal radiation dose. J. Nucl. Med. 40, 62S–101S.
Braem, A., Chamizo Llatas, M., Chesi, E., Correia, J.G., Garibaldi, F., et al., 2004. Feasibility of a novel design of high-resolution parallax-free Compton enhanced PET scanner dedicated to brain research. Phys. Med. Biol. 49, 2547–2562.
Brett, M., Leff, A.P., Rorden, C., Ashburner, J., 2001. Spatial normalization of brain images with focal lesions using cost function masking. NeuroImage 14, 486–500.
Bromiley, A., Welch, A., Chilcott, F., Waikar, S., McCallum, S., et al., 2001. Attenuation correction in PET using consistency conditions and a three-dimensional template. IEEE Trans. Nucl. Sci. 48, 1371–1377.
Bronnikov, A.V., 1999. Numerical solution of the identification problem for the attenuated Radon transform. Inverse Problems 15, 1315–1324.
Bronnikov, A.V., 2000. Reconstruction of attenuation map using discrete consistency conditions. IEEE Trans. Med. Imag. 19, 451–462.
Burger, C., Goerres, G., Schoenes, S., Buck, A., Lonn, A.H., et al., 2002. PET attenuation coefficients from CT images: experimental evaluation of the transformation of CT into PET 511-keV attenuation coefficients. Eur. J. Nucl. Med. Mol. Imaging 29, 922–927.
Carney, J., Beyer, T., Brasse, D., Yap, J.T., Townsend, D.W., 2002. CT-based attenuation correction for PET/CT scanners in the presence of contrast agent. Nuclear Science Symposium Conference Record, 2002 IEEE, pp. 1443–1446.
Carroll, L.R., Kretz, P., Orcutt, G., 1983. The orbiting rod source: Improving performance in PET transmission correction scans. In: Esser, P. (Ed.), Emission Computed Tomography: Current Trends The Society of Nuclear Medicine, pp. 235–247.
Carson, R.E., Daube-Witherspoon, M.E., Green, M.V., 1988. A method for postinjection PET transmission measurements with a rotating source. J. Nucl. Med. 29, 1558–1567.
Censor, Y., Gustafson, D., Lent, A., Tuy, H., 1979. A new approach to the emission computerized tomography problem: simultaneous calculation of attenuation and activity coefficients. IEEE Trans. Nucl. Sci. 26, 2275–2279.
Chao, T.-c., Xu, X.G., 2004. *S*-values calculated from a tomographic head/brain model for brain imaging. Phys. Med. Biol. 49, 4971–4984.
Collins, D.L., Zijdenbos, A.P., Kollokian, V., Sled, J.G., Kabani, N.J., et al., 1998. Design and construction of a realistic digital brain phantom. IEEE Trans. Med. Imag. 17, 463–468.
Comtat, C., Kinahan, P.E., Defrise, M., Michel, C., Townsend, D.W., 1998. Fast reconstruction of 3D PET data with accurate statistical modeling. IEEE Trans. Nucl. Sci. 45, 1083–1089.
Dahlbom, M., Hoffman, E., 1987. Problems in signal-to-noise ratio for attenuation correction in high resolution PET. IEEE Trans. Nucl. Sci. 34, 288–293.
Daube-Witherspoon, M., Carson, R.E., Green, M.V., 1988. Post-injection transmission attenuation measurements for PET. IEEE Trans. Nucl. Sci. 35, 757–761.
de Jong, H.W.A.M., Boellaard, R., Lenox, M., Michel, C., Lammertsma, A.A., 2004. Correction for emission contamination in transmission scans for the high resolution research tomograph. IEEE Trans. Nucl. Sci. 51, 673–676.
deKemp, R.A., Nahmias, C., 1994. Attenuation correction in PET using single photon transmission measurement. Med. Phys. 21, 771–778.
Deloar, H.M., Fujiwara, T., Shidahara, M., Nakamura, T., Watabe, H., et al., 1998. Estimation of absorbed dose for 2-[F-18]fluoro-2-deoxy-D-glucose using whole-body positron emission tomography and magnetic resonance imaging. Eur. J. Nucl. Med. 25, 565–574.
De Man, B., Nuyts, J., Dupont, P., Marchal, G., Suetens, P., 2000. Reduction of metal streak artifacts in X-ray computed tomography using a transmission maximum a posteriori algorithm. IEEE Trans. Nucl. Sci. 47, 977–981.
Demirkaya, O., 2002. Anisotropic diffusion filtering of PET attenuation data to improve emission images. Phys. Med. Biol. 47, N271–N278.
Dicken, V., 1999. A new approach towards simultaneous activity and attenuation reconstruction in emission tomography. Inverse Problems 15, 931–960.
Dogdas, B., Shattuck, D.W., Leahy, R.M., 2005. Segmentation of skull and scalp in 3-D human MRI using mathematical morphology. Hum. Brain Mapp. 26, 273–285.
El Fakhri, G., Kijewski, M.F., Johnson, K.A., Syrkin, G., Killiany, R.J., et al., 2003. MRI-guided SPECT perfusion measures and volumetric MRI in prodromal Alzheimer disease. Arch. Neurol. 60, 1066–1072.
Fessler, J.A., Ficaro, E.P., Clinthorne, N.H., Lange, K., 1997. Grouped-coordinate ascent algorithms for penalized-likelihood transmission image reconstruction. IEEE Trans. Med. Imag. 16, 166–175.
Fleming, J.S., 1989. A technique for using CT images in attenuation correction and quantification in SPECT. Nucl. Med. Commun. 10, 83–97.
Fowler, J.S., Volkow, N.D., Wang, G.J., Ding, Y.S., 2004. 2-Deoxy-2-[18F] fluoro-D-glucose and alternative radiotracers for positron emission tomography imaging using the human brain as a model. Semin. Nucl. Med. 34, 112–121.
Freedman, N.M., Bacharach, S.L., Carson, R.E., Price, J.C., Dilsizian, V., 1996. Effect of smoothing during transmission processing on quantitative cardiac PET scans. J. Nucl. Med. 37, 690–694.
Gilman, S., 1998. Imaging the brain. First of two parts. N. Engl. J. Med. 338, 812–820.
Glatting, G., Wuchenauer, M., Reske, S.N., 2000. Simultaneous iterative reconstruction for emission and attenuation images in positron emission tomography. Med. Phys. 27, 2065–2071.
Goerres, G.W., Hany, T.F., Kamel, E., von Schulthess, G.K., Buck, A., 2002. Head and neck imaging with PET and PET/CT: artefacts from dental metallic implants. Eur. J. Nucl. Med. Mol. Imaging 29, 367–370.
Greitz, T., Bohm, C., Holte, S., Eriksson, L., 1991. A computerized brain atlas: construction, anatomical content, and some applications. J. Comput. Assist. Tomogr. 15, 26–38.
Gunn, R.N., Lammertsma, A.A., Hume, S.P., Cunningham, V.J., 1997.

Parametric imaging of ligand–receptor binding in PET using a simplified reference region model. NeuroImage 6, 279–287.
Guy, M.J., Castellano-Smith, I.A., Flower, M.A., Flux, G.D., Ott, R.J., et al., 1998. DETECT–dual energy transmission estimation CT–for improved attenuation correction in SPECT and PET. IEEE Trans. Nucl. Sci. 45, 1261–1267.
Hasegawa, B., Zaidi, H., 2005. Dual-modality imaging: more than the sum of its components. In: Zaidi, H. (Ed.), Quantitative Analysis in Nuclear Medicine Imaging. Springer, New York, pp. 35–81.
Heiss, W.-D., Herholz, K., 2006. Brain receptor imaging. J. Nucl. Med. 47, 302–312.
Heller, G.V., Links, J., Bateman, T.M., Ziffer, J.A., Ficaro, E., et al., 2004. American society of nuclear cardiology and society of nuclear medicine joint position statement: attenuation correction of myocardial perfusion SPECT scintigraphy. J. Nucl. Cardiol. 11, 229–230.
Hoffman, E.J., Cutler, P.D., Digby, W.M., Mazziotta, J.C., 1990. 3-D phantom to simulate cerebral blood flow and metabolic images for PET. IEEE Trans. Nucl. Sci. 37, 616–620.
Hooper, P.K., Meikle, S.R., Eberl, S., Fulham, M.J., 1996. Validation of postinjection transmission measurements for attenuation correction in neurological FDG-PET studies. J. Nucl. Med. 37, 128–136.
Hosaka, K., Ishii, K., Sakamoto, S., Sadato, N., Fukuda, H., et al., 2005. Validation of anatomical standardization of FDG PET images of normal brain: comparison of SPM and NEUROSTAT. Eur. J. Nucl. Med. Mol. Imaging 32, 92–97.
Huang, S.C., Hoffman, E.J., Phelps, M.E., Kuhl, D.E., 1979. Quantitation in positron emission computed tomography: 2. Effects of inaccurate attenuation correction. J. Comput. Assist. Tomogr. 3, 804–814.
Huang, S.C., Carson, R.E., Phelps, M.E., Hoffman, E.J., Schelbert, H.R., et al., 1981. A boundary method for attenuation correction in positron computed tomography. J. Nucl. Med. 22, 627–637.
Huesman, R., Derenzo, S.E., Cahoon, J.L., Geyer, A.B., Moses, W.W., et al., 1988. Orbiting transmission source for positron tomography. IEEE Trans. Nucl. Sci. 35, 735–739.
Hustinx, R., Dolin, R.J., Benard, F., Bhatnagar, A., Chakraborty, D., et al., 2000. Impact of attenuation correction on the accuracy of FDG-PET in patients with abdominal tumors: a free-response ROC analysis. Eur. J. Nucl. Med. 27, 1365–1371.
Hutton, B.F., Braun, M., 2003. Software for image registration: algorithms, accuracy, efficacy. Semin. Nucl. Med. 33, 180–192.
ICRU, . Tissue substitutes in radiation dosimetry and measurement. Report 44 (International Commission on Radiological Units and Measurements (ICRU), Bethesda, MD).
Jacobs, A.H., Li, H., Winkeler, A., Hilker, R., Knoess, C., et al., 2003. PET-based molecular imaging in neuroscience. Eur. J. Nucl. Med. Mol. Imaging 30, 1051–1065.
Jones, W.F., Digby, W.M., Luk, W.K., Casey, M.E., Byars, L.G., 1995. Optimizing rod window width in positron emission tomography. IEEE Trans. Med. Imag. 14, 266–270.
Kamel, E., Hany, T.F., Burger, C., Treyer, V., Lonn, A.H., et al., 2002. CT vs 68Ge attenuation correction in a combined PET/CT system: evaluation of the effect of lowering the CT tube current. Eur. J. Nucl. Med. Mol. Imaging 29, 346–350.
Kamel, E.M., Burger, C., Buck, A., von Schulthess, G.K., Goerres, G.W., 2003. Impact of metallic dental implants on CT-based attenuation correction in a combined PET/CT scanner. Eur. Radiol. 13, 724–728.
Kaneko, K., Kuwabara, Y., Sasaki, M., Koga, H., Abe, K., et al., 2004. Validation of quantitative accuracy of the post-injection transmission-based and transmissionless attenuation correction techniques in neurological FDG-PET. Nucl. Med. Commun. 25, 1095–1102.
Kaplan, M.S., Haynor, D.R., Vija, H., 1999. A differential attenuation method for simultaneous estimation of SPECT activity and attenuation distributions. IEEE Trans. Nucl. Sci. 46, 535–541.
Karp, J.S., Muehllehner, G., Qu, H., Yan, X.H., 1995. Singles transmission in volume-imaging PET with a 137Cs source. Phys. Med. Biol. 40, 929–944.
Kinahan, P.E., Townsend, D.W., Beyer, T., Sashin, D., 1998. Attenuation correction for a combined 3D PET/CT scanner. Med. Phys. 25, 2046–2053.
Kinahan, P.E., Hasegawa, B., Beyer, T., 2003a. X-ray-based attenuation correction for positron emission tomography/computed tomography scanners. Semin. Nucl. Med. 34, 166–179.
Kinahan, P.E., Hasegawa, B.H., Beyer, T., 2003b. X-ray-based attenuation correction for positron emission tomography/computed tomography scanners. Semin. Nucl. Med. 33, 166–179.
Kitamura, K., Iida, H., Shidahara, M., Miura, S., Kanno, I., 2000. Noise reduction in PET attenuation correction using non-linear Gaussian filters. IEEE Trans. Nucl. Sci. 47, 994–999.
Krol, A., Bowsher, J.E., Manglos, S.H., Feiglin, D.H., Tornai, M.P., et al., 2001. An EM algorithm for estimating SPECT emission and transmission parameters from emissions data only. IEEE Trans. Med. Imag. 20, 218–232.
Kubler, W., Ostertag, H., Hoverath, H., Doll, J., Ziegler, S., et al., 1988. Scatter suppression by using a rotating pin source in PET transmission measurements. IEEE Trans. Nucl. Sci. 35, 749–752.
Kwan, R.K.-S., Evans, A.C., Pike, G.B., 1999. MRI simulation-based evaluation of image-processing and classification methods. IEEE Trans. Med. Imag. 18, 1085–1097.
LaCroix, K.J., Tsui, B.M.W., Hasegawa, B.H., Brown, J.K., 1994. Investigation of the use of X-ray CT images for attenuation compensation in SPECT. IEEE Trans. Nucl. Sci. 41, 2793–2799.
Lammertsma, A.A., Hume, S.P., 1996. Simplified reference tissue model for PET receptor studies. NeuroImage 4, 153–158.
Lammertsma, A.A., Heather, J.D., Jones, T., Frackowiak, R.S., Lenzi, G.L., 1982. A statistical study of the steady state technique for measuring regional cerebral blood flow and oxygen utilisation using 15O. J. Comput. Assist. Tomogr. 6, 566–573.
Larsson, S.A., Jonsson, C., Pagani, M., Johansson, L., Jacobsson, H., 2000. A novel phantom design for emission tomography enabling scatter- and attenuation-"free" single-photon emission tomography imaging. Eur. J. Nucl. Med. 27, 131–139.
Lartizien, C., Kinahan, P.E., Swensson, R., Comtat, C., Lin, M., et al., 2003. Evaluating image reconstruction methods for tumor detection in 3-dimensional whole-body PET oncology imaging. J. Nucl. Med. 44, 276–290.
Lodge, M.A., Badawi, R.D., Marsden, P.K., 1998. A clinical evaluation of the quantitative accuracy of simultaneous emission/transmission scanning in whole-body positron emission tomography. Eur. J. Nucl. Med. 25, 417–423.
Luk, W.R., Digby, W.D., Jones, W.F., Casey, M.E., 1995. An analysis of correction methods for emission contamination in PET postinjection transmission measurement. IEEE Trans. Nucl. Sci. 42, 2303–2308.
Ma, Y., Kamber, M., Evans, A.C., 1993. 3D simulation of PET brain images using segmented MRI data and positron tomograph characteristics. Comput. Med. Imaging Graph 17, 365–371.
Mahnken, A.H., Raupach, R., Wildberger, J.E., Jung, B., Heussen, N., et al., 2003. A new algorithm for metal artifact reduction in computed tomography: in vitro and in vivo evaluation after total hip replacement. Invest. Radiol. 38, 769–775.
Marsden, P.K., Strul, D., Keevil, S.F., Williams, S.C., Cash, D., 2002. Simultaneous PET and NMR. Br. J. Radiol. 75 Spec No, S53–S59.
Meikle, S.R., Dahlbom, M., Cherry, S.R., 1993. Attenuation correction using count-limited transmission data in positron emission tomography. J. Nucl. Med. 34, 143–150.
Meikle, S.R., Bailey, D.L., Hooper, P.K., Eberl, S., Hutton, B.F., et al., 1995. Simultaneous emission and transmission measurements for attenuation correction in whole-body PET. J. Nucl. Med. 36, 1680–1688.
Meikle, S.R., Eberl, S., Hooper, P.K., Fulham, M.J., 1997. Simultaneous emission and transmission (SET) scanning in neurological PET studies. J. Comput. Assist. Tomogr. 21, 487–497.
Mesina, C.T., Boellaard, R., van den Heuvel, O.A., Veltman, D.J., Jongbloed, G., et al., 2003. Effects of attenuation correction and reconstruction method on PET activation studies. NeuroImage 20, 898–908.
Michel, C., Bol, A., De_Volder, A.G., Goffinet, A.M., 1989. Online brain

attenuation correction in PET: towards a fully automated data handling in a clinical environment. Eur. J. Nucl. Med. 15, 712–718.
Montandon, M.-L., 2005. Quantification of three-dimensional positron emission tomography images. PhD thesis, Geneva University, Geneva.
Montandon, M.-L., Zaidi, H., 2005. Atlas-guided non-uniform attenuation correction in cerebral 3D PET imaging. NeuroImage 25, 278–286.
Montandon, M.-L., Zaidi, H., in press. Quantitative VOI-based analysis of template-based attenuation correction in 3D brain PET. Comput. Med. Imaging Grap. doi:10.1016/j.compmedimag.2006.09.017.
Montandon, M.-L., Slosman, D.O., Zaidi, H., 2003. Assessment of the impact of model-based scatter correction on 18F-[FDG] 3D brain PET in healthy subjects using statistical parametric mapping. NeuroImage 20, 1848–1856.
Nakamoto, Y., Chin, B.B., Kraitchman, D.L., Lawler, L.P., Marshall, L.T., et al., 2003. Effects of nonionic intravenous contrast agents at PET/CT imaging: phantom and canine studies. Radiology 227, 817–824.
Natterer, F., 1993. Determination of tissue attenuation in emission tomography of optically dense media. Inverse Problems 9, 731–736.
Natterer, F., 2001. Inversion of the attenuated Radon transform. Inverse Problems 17, 113–119.
Nehmeh, S.A., Erdi, Y.E., Kalaigian, H., Kolbert, K.S., Pan, T., et al., 2003. Correction for oral contrast artifacts in CT attenuation-corrected PET images obtained by combined PET/CT. J. Nucl. Med. 44, 1940–1944.
Nickoloff, E.L., Perman, W.H., Esser, P.D., Bashist, B., Alderson, P.O., 1984. Left ventricular volume: physical basis for attenuation corrections in radionuclide determinations. Radiology 152, 511–515.
Novikov, R.G., 2002. An inversion formula for the attenuated X-ray transformation. Ark. Mat. 40, 145–167.
Nuyts, J., Dupont, P., Stroobants, S., Benninck, R., Mortelmans, L., et al., 1999. Simultaneous maximum a posteriori reconstruction of attenuation and activity distributions from emission sinograms. IEEE Trans. Med. Imag. 18, 393–403.
Osman, M.M., Cohade, C., Nakamoto, Y., Wahl, R.L., 2003. Respiratory motion artifacts on PET emission images obtained using CT attenuation correction on PET-CT. Eur. J. Nucl. Med. Mol. Imaging 30, 603–606.
Ostertag, H., Kubler, W.K., Doll, J., Lorenz, W.J., 1989. Measured attenuation correction methods. Eur. J. Nucl. Med. 15, 722–726.
Palmer, M.R., Rogers, J.G., Bergstrom, M., Beddoes, M.P., Pate, B.D., 1986. Transmission profile filtering for positron emission tomography. IEEE Trans. Nucl. Sci. 33, 478–481.
Panin, V.Y., Kehren, F., Hamill, J., Michel, C., 2004. Application of discrete data consistency conditions for selecting regularization parameters in PET attenuation map reconstruction. Phys. Med. Biol. 49, 2425–2436.
Phelps, M.E., Huang, S.C., Hoffman, E.J., Selin, C., Sokoloff, L., et al., 1979. Tomographic measurement of local cerebral glucose metabolic rate in humans with (F-18)2-fluoro-2-deoxy-D-glucose: validation of method. Ann. Neurol. 6, 371–388.
Ranger, N.T., Thompson, C.J., Evans, A.C., 1989. The application of a masked orbiting transmission source for attenuation correction in PET. J. Nucl. Med. 30, 1056–1068.
Reilhac, A., Batan, G., Michel, C., Grova, C., Tohka, J., et al., 2005. PET-SORTEO: validation and development of database of simulated PET volumes. IEEE Trans. Nucl. Sci. 52, 1321–1328.
Riddell, C., Brigger, P., Carson, R.E., Bacharach, S., 1999. The watershed algorithm: a method to segment noisy PET transmission images. IEEE Trans. Nucl. Sci. 46, 713–719.
Rousset, O.G., Ma, Y., Evans, A.C., 1998. Correction for partial volume effects in PET: principle and validation. J. Nucl. Med. 39, 904–911.
Seguinot, J., Braem, A., Chesi, E., Joram, C., Mathot, S., et al., 2006. Novel geometrical concept of high performance brain PET scanner: Principle, design and performance estimates. Nuovo Cimento C 29, 429–463.
Setani, K., Schreckenberger, M., Sabri, O., Meyer, P.T., Zeggel, T., et al., 2000. Comparison of different methods for attenuation correction in brain PET: effect on the calculation of the metabolic rate of glucose. Nuklearmedizin 39, 50–55 (German).
Siegel, S., Dahlbom, M., 1992. Implementation and evaluation of a calculated attenuation correction for PET. IEEE Trans. Nucl. Sci. 39, 1117–1121.
Siewerdsen, J.H., Daly, M.J., Bakhtiar, B., Moseley, D.J., Richard, S., et al., 2006. A simple, direct method for X-ray scatter estimation and correction in digital radiography and cone-beam CT. Med. Phys. 33, 187–197.
Slifstein, M., Hwang, D.R., Martinez, D., Ekelund, J., Huang, Y., et al., 2006. Biodistribution and radiation dosimetry of the dopamine D2 ligand 11C-raclopride determined from human whole-body PET. J. Nucl. Med. 47, 313–319.
Sokoloff, L., Reivich, M., Kennedy, C., Des Rosiers, M.H., Patlak, C.S., et al., 1977. The [^{14}C]deoxyglucose method for the measurement of local cerebral glucose utilization: theory, procedure, and normal values in the conscious and anesthetized albino rat. J. Neurochem. 28, 897–916.
Sossi, V., Camborde, M.L., Tropini, G., Newport, D., Rahmim, A., et al., 2005. The influence of measurement uncertainties on the evaluation of the distribution volume ratio and binding potential in rat studies on a microPET R4: a phantom study. Phys. Med. Biol. 50, 2859–2869.
Spitzer, V.M., Whitlock, D.G., 1998. The visible human dataset: the anatomical platform for human simulation. Anat. Rec. 253, 49–57.
Stamatakis, E.A., Wilson, J.T., Wyper, D.J., 2001. Using lesion masking to facilitate nonlinear alignment of SPECT images. NeuroImage 13, S42.
Stodilka, R.Z., Kemp, B.J., Prato, F.S., Kertesz, A., Kuhl, D., et al., 2000. Scatter and attenuation correction for brain SPECT using attenuation distributions inferred from a head atlas. J. Nucl. Med. 41, 1569–1578.
Tai, Y.-C., Lin, K.-P., Dahlbom, M., Hoffman, E., 1996. A hybrid attenuation correction technique to compensate for lung density in 3-D total body PET. IEEE Trans. Nucl. Sci. 43, 323–330.
Tang, H.R., Brown, J.K., Da Silva, A.J., Matthay, K.K., Price, D.C., et al., 1999. Implementation of a combined X-ray CT-scintillation camera imaging system for localizing and measuring radionuclide uptake: experiments in phantoms and patients. IEEE Trans. Nucl. Sci. 46, 551–557.
Tellmann, L., Fulton, R., Pietrzyk, U., Nickel, I., Stangier, I., et al., 2006. Concepts of registration and correction of head motion in positron emission tomography. Z. Med. Phys. 16, 67–74.
Thompson, C.J., Ranger, N., Evans, A.C., Gjedde, A., 1991. Validation of simultaneous PET emission and transmission scans. J. Nucl. Med. 32, 154–160.
Tomitani, T., 1987. An edge detection algorithm for attenuation correction in emission CT. IEEE Trans. Nucl. Sci. 34, 309–312.
Townsend, D.W., Cherry, S.R., 2001. Combining anatomy and function: the path to true image fusion. Eur. Radiol. 11, 1968–1974.
Townsend, D.W., Carney, J.P.J., Yap, J.T., Hall, N.C., 2004. PET/CT today and tomorrow. J. Nucl. Med. 45, 4s–14s.
van den Heuvel, O.A., Boellaard, R., Veltman, D.J., Mesina, C., Lammertsma, A.A., 2003. Attenuation correction of PET activation studies in the presence of task-related motion. NeuroImage 19, 1501–1509.
Van Laere, K., Zaidi, H., 2005. Quantitative analysis in functional brain imaging. In: Zaidi, H. (Ed.), Quantitative Analysis in Nuclear Medicine Imaging. Springer, New York, pp. 435–470.
Van Laere, K., Koole, M., Kauppinen, T., Monsieurs, M., Bouwens, L., et al., 2000. Nonuniform transmission in brain SPECT using 201Tl, 153Gd, and 99 mTc static line sources: anthropomorphic dosimetry studies and influence on brain quantification. J. Nucl. Med. 41, 2051–2062.
Wahl, R.L., 1999. To AC or not to AC: that is the question. J. Nucl. Med. 40, 2025–2028 [editorial].
Wang, G., Frei, T., Vannier, M.W., 2000. Fast iterative algorithm for metal artifact reduction in X-ray CT. Acad. Radiol. 7, 607–614.
Watabe, H., Sato, N., Deloar, H.M., Urayama, S.I., Oka, H., et al., 2001. Acquisition of attenuation map for brain PET study using optical tracking system. Proc. IEEE Nuclear Science Symposium and Medical Imaging Conference, San Diego, CA, pp. 1458–1461.
Watson, C.C., Schaefer, A., Luk, W.K., Kirsch, C.M., 1999. Clinical evaluation of single-photon attenuation correction for 3D whole-body PET. IEEE Trans. Nucl. Sci. 46, 1024–1031.
Watson, C.C., Eriksson, L., Casey, M.E., Jones, W.F., Moyers, J.C., et al.,

2001. Design and performance of collimated coincidence point sources for simultaneous transmission measurements in 3-D PET. IEEE Trans. Nucl. Sci. 48, 673–679.

Weinzapfel, B.T., Hutchins, G.D., 2001. Automated PET attenuation correction model for functional brain imaging. J. Nucl. Med. 42, 483–491.

Welch, A., Campbell, C., Clackdoyle, R., Natterer, F., Hudson, M., et al., 1998. Attenuation correction in PET using consistency information. IEEE Trans. Nucl. Sci. 45, 3134–3141.

Welch, A., Hallett, W., Marsden, P., Bromiley, A., 2003. Accurate attenuation correction in PET using short transmission scans and consistency information. IEEE Trans. Nucl. Sci. 50, 427–432.

Wu, T.-H., Huang, Y.-H., Lee, J.S., Wang, S.-Y., Wang, S.-C., et al., 2004. Radiation exposure during transmission measurements: comparison between CT- and germanium-based techniques with a current PET scanner. Eur. J. Nucl. Med. Mol. Imaging 31, 38–43.

Xu, M., Cutler, P., Luk, W., 1996. Adaptive, segmented attenuation correction for whole-body PET imaging. IEEE Trans. Nucl. Sci. 43, 331–336.

Xu, X.G., Chao, T.C., Bozkurt, A., 2000. VIP-Man: an image-based whole-body adult male model constructed from color photographs of the Visible Human Project for multi-particle Monte Carlo calculations. Health Phys. 78, 476–486.

Yu, S.K., Nahmias, C., 1996. Segmented attenuation correction using artificial neural networks in positron tomography. Phys. Med. Biol. 41, 2189–2206.

Zaidi, H., 1999. Relevance of accurate Monte Carlo modeling in nuclear medical imaging. Med. Phys. 26, 574–608.

Zaidi, H., Hasegawa, B.H., 2003. Determination of the attenuation map in emission tomography. J. Nucl. Med. 44, 291–315.

Zaidi, H., Koral, K.F., 2004. Scatter modelling and compensation in emission tomography. Eur. J. Nucl. Med. Mol. Imaging 31, 761–782.

Zaidi, H., Montandon, M.-L., 2006. The new challenges of brain PET imaging technology. Curr. Med. Imag. Rev. 2, 3–13.

Zaidi, H., Sossi, V., 2004. Correction for image degrading factors is essential for accurate quantification of brain function using PET. Med. Phys. 31, 423–426.

Zaidi, H., Laemmli, C., Allaoua, M., Gries, P., Slosman, D.O., 2001. Optimizing attenuation correction in clinical cerebral 3D PET: which method to use? J. Nucl. Med. 42, 195–196.

Zaidi, H., Diaz-Gomez, M., Boudraa, A.E., Slosman, D.O., 2002. Fuzzy clustering-based segmented attenuation correction in whole-body PET imaging. Phys. Med. Biol. 47, 1143–1160.

Zaidi, H., Montandon, M.-L., Slosman, D.O., 2003. Magnetic resonance imaging-guided attenuation and scatter corrections in three-dimensional brain positron emission tomography. Med. Phys. 30, 937–948.

Zaidi, H., Montandon, M.-L., Slosman, D.O., 2004. Attenuation compensation in cerebral 3D PET: effect of the attenuation map on absolute and relative quantitation. Eur. J. Nucl. Med. Mol. Imaging 31, 52–63.

Zhao, S., Robertson, D.D., Wang, G., Whiting, B., Bae, K.T., 2000. X-ray CT metal artifact reduction using wavelets: an application for imaging total hip prostheses. IEEE Trans. Med. Imag. 19, 1238–1247.

Zubal, I.G., Harrell, C.R., Smith, E.O., Rattner, Z., Gindi, G., et al., 1994. Computerized 3-dimensional segmented human anatomy. Med. Phys. 21, 299–302.